Bottom-Up Approach for the Rational Loading of Linear Oligomers and Polymers with Lanthanides

Mirzakhani, Mohsen; Nozary, Homayoun; Naseri, Soroush; Besnard, Céline; Guenee, Laure; Piguet, Claude

How to cite

MIRZAKHANI, Mohsen et al. Bottom-Up Approach for the Rational Loading of Linear Oligomers and Polymers with Lanthanides. In: Inorganic chemistry, 2021, vol. 60, n° 20, p. 15529–15542. doi: 10.1021/acs.inorgchem.1c02157

This publication URL: https://archive-ouverte.unige.ch/unige:155854
Publication DOI: 10.1021/acs.inorgchem.1c02157

Publication: *Inorg. Chem.* **2021**, *60*, 15529-15542. DOI: 10.1021/acs.inorgchem.1c02157

A Bottom Up Approach for the Rational Loading of Linear Oligomers and Polymers with Lanthanides

Mohsen Mirzakhani,[a] Homayoun Nozary,[a] Soroush Naseri,[a] Céline Besnard,[b] Laure Guénée[b] and Claude Piguet [a,*]

[a] *Department of Inorganic and Analytical Chemistry. University of Geneva, 30 quai E. Ansermet CH-1211 Geneva 4 (Switzerland).*

[b] *Laboratory of Crystallography. University of Geneva, 24 quai E. Ansermet. CH-1211 Geneva 4 (Switzerland).*

[*]Email: claude.piguet@unige.ch

ABSTRACT: The adducts between luminescent lanthanide tris-β-diketonates and diimine or triimine ligands have been explored exhaustively for their exceptional photophysical properties. Their formation, stability and structures in solution together with the design of extended metallopolymers exploiting these building blocks remain however elusive. The systematic peripheral substitution of tridentate 2,6-bis(benzimidazol-2-yl)pyridine binding units (**L*k*** = **L1**-**L5**), taken as building blocks for linear oligomers and polymers, allows a fine tuning of their affinity toward neutral [Ln(hfa)$_3$] lanthanide containers (hfa = hexafluoroacateylacetone) in the [**L*k***Ln(hfa)$_3$] adducts. Two trends emerge with (i) an unusual pronounced thermodynamic selectivity for mid-range lanthanides (Ln = Eu) and (ii) an intriguing influence of remote peripheral substitutions of the benzimidazole rings on the affinity of the tridentate unit for [Ln(hfa)$_3$]. These trends are amplified upon connecting several tridentate binding units via their benzimidazole rings to give linear segmental dimers (**L6**) and trimers (**L7**), which are considered as models for programming linear Wolf-Type II metallopollymers. The modulation of the affinity between the terminal and central binding units in the linear multi-tridentate ligands deciphers the global decrease of metal-ligand binding strengths with the increasing length of the receptors (monomer $\rightarrow$ dimer $\rightarrow$ trimer $\rightarrow$ polymer). Application of the site binding model shed light on the origin of the variation of the thermodynamic affinities: a prerequisite for the programmed

loading of polymer backbone with luminescent lanthanide β-diketonates. The analysis of crystal structures for these adducts reveals delicate correlations between chemical bond lengths measured in the solid state (or bond valence parameters) and metal-ligand affinities operating in solution.

Introduction

Since more than a century, organic (bio)polymers and macromolecules with increasing sizes and complexities are at the front of the design and applications of chemical materials.[1] The 1953 Nobel prize, attributed to Staudinger for *his discoveries in the field of macromolecular chemistry*, officially recognized (bio)polymers as a crucial field in (bio)chemistry,[2] which rapidly led to countless technological developments in view of their easy processability, efficient structural control, adjustable mechanical properties and rich scalability.[3] Some recent improvements in the understanding and control of weak intermolecular interactions have opened new areas, in which supramolecular concepts have been exploited for further enriching the (bio)polymers domain.[4] In term of electronic, optical and magnetic properties, organic (bio)polymers are limited by their closed-shell atomic constituents. The introduction of open-shell d-block or f-block elements provides metallopolymers or hybrid materials[5] which can be exploited for promising applications in light-emitting diodes (LED),[6] in solid cells for photovoltaics,[7] in magnetically-active[8] and light-emissive layers,[9] in telecommunication devices[10] and in temperature sensing.[11] Among the possible arrangements of the metal complexes with respect to the polymer backbone,[12] referred to as Wolf-Type I, Type II and Type III (Scheme 1a),[5a,13] only the Type III polymers, in which a stochiometric amount of metals is part of the polymeric backbone, have been intensively investigated in inorganic chemisty. They are commonly designed as functional coordination polymers[7c,9a,14] or metal-organic frameworks (MOF).[15] On the other hand, only limited efforts have been focused on the rational thermodynamic metal loading of predefined polymeric organic receptors to give Type I and Type II metallopolymers with well-defined compositions and structures.[16] This appears all the more surprising that a simple thermodynamic approach, i.e. the site binding model, has been specifically

developped for catching the energy changes accompanying the multi-site protonation[17] or complexation[18] of linear polymers **P** (equilibrium 1).

$$\mathbf{P} \quad + \quad m\mathrm{M} \quad \rightleftharpoons \quad [\mathbf{P}\mathrm{M}_m] \qquad \Delta G_{m,1}^{\mathrm{M,P}} = -RT\ln\left(\beta_{m,1}^{\mathrm{M,P}}\right) \qquad (1)$$

The basic concept relies on the interpretation of the accessible macroscopic stability constants $\beta_{m,1}^{\mathrm{M,P}}$ in term of only two easy-to-interpret parameters (i) the intrinsic metal-binding site affinity $f_i^{\mathrm{M,P}}$, which is characteristic for a single host-guest interaction ($\Delta G_{\mathrm{aff},i}^{\mathrm{M,P}} = -RT\ln\left(f_i^{\mathrm{M,P}}\right)$), and (ii) the cooperativity factor $u_{1-2}^{\mathrm{M,M}}$ which gauges the free energy of inter-guest interaction when two next host-sites are occupied ($\Delta E_{1\text{-}2}^{\mathrm{M,M}} = -RT\ln\left(u_{1-2}^{\mathrm{M,M}}\right)$, Scheme 1b).

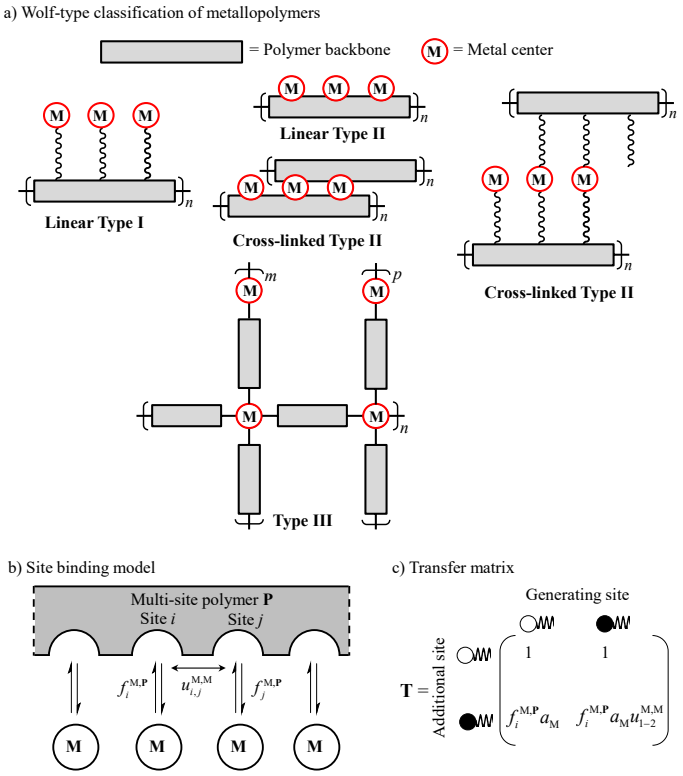

Scheme 1 a) Classifications of metallopolymers according to Wolf.[5a,13] b) Thermodynamic model for rationalizing the successive intermolecular connections of guests (M) to a one-dimensional multi-site polymer (**P**). $\Delta G_{\mathrm{aff},i}^{\mathrm{M,P}} = -RT\ln\left(f_i^{\mathrm{M,P}}\right)$ is the free energy of intermolecular metal-binding site affinity and $\Delta E_{i\text{-}j}^{\mathrm{M,M}} = -RT\ln\left(u_{i\text{-}j}^{\mathrm{M,M}}\right)$ is the free energy of intermetallic interaction. c) Transfer matrix **T** adapted to the metal loading of a linear polymeric receptor with intersite interactions limited to nearest-neighbours (a_{M} is the metal activity).[17,18]

In term of statistical mechanics, the relevant information on the binding properties of metal M to a linear polymer **P** with *N* binding site is contained in the semi-grand canonical partition function Ξ. The latter can be expanded in terms of the metal activities a_{M} with the help of the transfer matrix formalism (Scheme 1c) to give the so-called binding polynomial (eqn 2).[16-18]

$$\Xi = \sum_{m=0}^{N} \beta_{m,1}^{\mathrm{M},\mathbf{P}} \left(a_{\mathrm{M}}\right)^{m} = \tilde{\mathrm{V}}_{\mathrm{t}}\, \mathbf{T}^{N}\, \mathrm{V}_{g} \qquad \text{with } \mathrm{V_g} = \begin{pmatrix} 1 \\ 0 \end{pmatrix} \text{ and } \tilde{\mathrm{V}}_{\mathrm{t}} = \begin{pmatrix} 1 & 1 \end{pmatrix} \tag{2}$$

Having intrisic affinity $f_i^{\mathrm{M},\mathbf{P}}$ and cooperativity factor $u_{1-2}^{\mathrm{M,M}}$ at hand, Ξ can be easily computed (eqn 2 and Scheme 1c) for various free metal activities a_{M}, from which the degree of metalation $\theta_{\mathrm{M}} = \langle m \rangle / N$, also known as the occupancy factor estimating the average of bound metals per available sites in the receptor, is obtained by derivation.

$$\theta_{\mathrm{M}} = \frac{\langle m \rangle}{N} = \frac{1}{N} \frac{d \ln(\Xi)}{d \ln(a_{\mathrm{M}})} = \frac{1}{N} \frac{\sum_{m=0}^{N} m \beta_{m,1}^{\mathrm{M},\mathbf{P}} \left(a_{\mathrm{M}}\right)^{m}}{\sum_{m=0}^{N} \beta_{m,1}^{\mathrm{M},\mathbf{P}} \left(a_{\mathrm{M}}\right)^{m}} = \frac{1}{N} \frac{|\mathrm{M}|_{\mathrm{bound}}}{|\mathbf{P}|_{\mathrm{tot}}} = \frac{1}{N} \frac{|\mathrm{M}|_{\mathrm{tot}} - |\mathrm{M}|}{|\mathbf{P}|_{\mathrm{tot}}} \tag{3}$$

Reasonably assuming that the molar concentration of free metal $|\mathrm{M}|$ can be taken as a good estimation of its activity ($a_{\mathrm{M}} = \gamma_{\mathrm{M}} |\mathrm{M}| \simeq |\mathrm{M}|$), the experimental occupancy factors θ_{M} measured for a series of solutions with different $\langle |\mathrm{M}|_{\mathrm{tot}} ; |\mathbf{P}|_{\mathrm{tot}} \rangle$ pairs (right part of eqn 3) can be compared with their theoretical counterparts (central part of eqn 3) in oder to extract an optimized set of marcoscopic formation constants $\beta_{m,1}^{\mathrm{M},\mathbf{P}}$ by using non-linear least-square fitting techniques. Introduction of the latter constants into eqn (2) gives intrinsic metal-binding site affinity $f_i^{\mathrm{M},\mathbf{P}}$ and intermetallic interaction parameter $u_{i,j}^{\mathrm{M,M}}$.

Applied to the loading of linear polymers $\mathbf{P1}^{N}$ of different lengths (N = 1-31) with [La(hfa)$_3$(dig)] (hfa = hexafluoroacetylacetonate, dig = diglyme = bis(2-methoxyethyl)ether) in dichloromethane solutions containing a total fixed diglyme concentration of $|\mathrm{dig}|_{\mathrm{tot}}$ = 0.14 M (Figure 1a), the latter procedure provided the conditional intrinsic affinities $f_{\mathrm{cond}}^{\mathrm{La},\mathbf{P1}^{N}}$ of one tridentate site in the polymer for

[La(hfa)$_3$] depicted in Figure 1b.[19] The surprising negative power dependence of $f_{cond}^{Ln,\mathbf{P1}^N}$ with the length of the polymer was tentatively assigned to some length-dependent freezing of the rotational degrees of freedom accompanying the successive fixation of an entering [Ln(hfa)$_3$] metal unit into the polymer.[20]

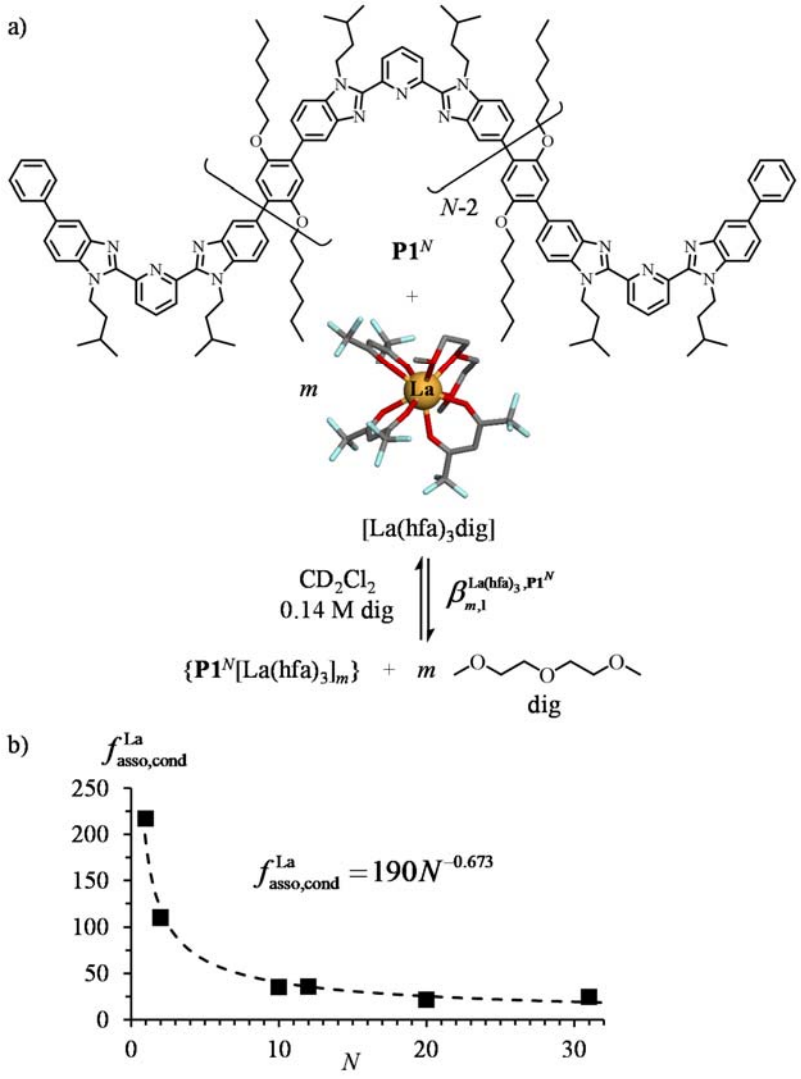

Figure 1 a) Host–guest association for the connection of [La(hfa)$_3$] containers to linear multi-tridentate polymers **P1**^{N} and b) average conditional intrinsic association affinity $f_{asso,cond}^{La}$ of a tridentate site in polymers **P1**^{N} (N = 1, 2, 10, 12, 20, 31) for [La(hfa)$_3$] (N is the number of available tridentate binding sites, CD_2Cl_2 + 0.14 M diglyme, 293 K).[19] Color code: C = grey, O = red, N = blue, F = light blue, La = orange, hydrogen atoms are omitted for clarity)

The subsequent discovery that the intrinsic affinities of [La(hfa)$_3$] for the monomers **M1**-**M4** indeed vary with the lipophilicity of the aromatic bridges, which are required for building the polymers **P1**^{N} (Figure 2), casts doubt on the original claim for pure structural effects induced by stiffening upon metal complexation.[21] Since this uncontrolled trend is harmful for (i) programming metallopolymers with rational metal affinities and (ii) extracting reliable cooperative factors, we propose here, once and for all, to rationally address the origin of the decreasing affinity of the binding site with the increasing length in these linear oligomers/polymers.

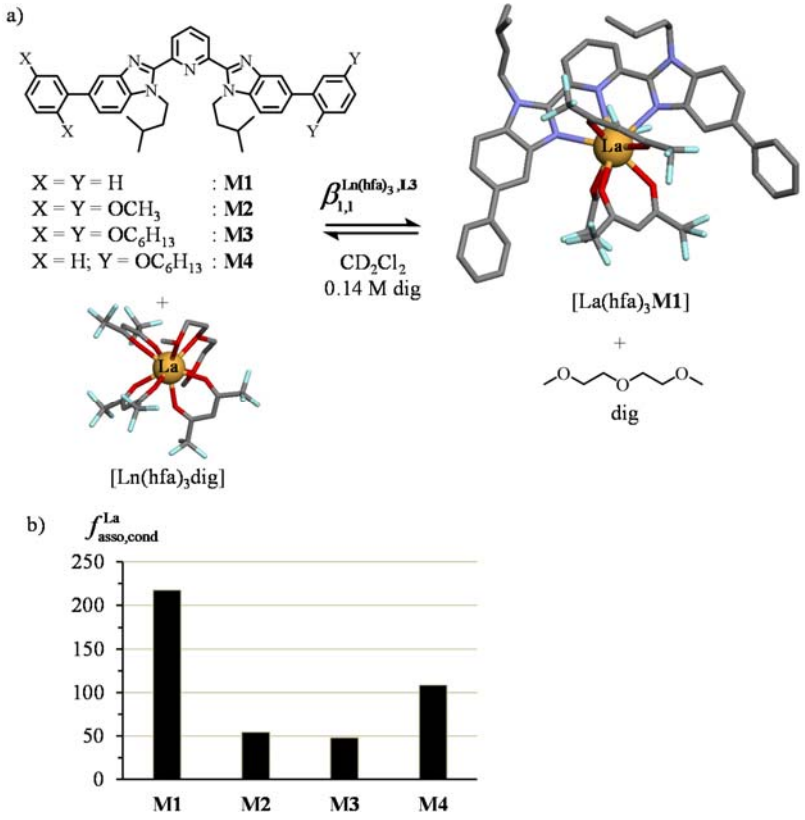

Figure 2 a) Host-guest association for the connection of the monomeric tridentate ligand **M1**-**M4** ligands to [Ln(hfa)$_3$] containers and b) average conditional intrinsic association affinity $f^{La}_{asso,cond}$ of the tridentate site in monomers **M1**-**M4** for [La(hfa)$_3$] (CD_2Cl_2 + 0.14 M diglyme, 293 K).[21] Color code: C = grey, O = red, N = blue, F = light blue, La = orange, hydrogen atoms are omitted for clarity)

In this context, the five receptors **L1**-**L5** have been designed for unravelling the influence of remote benzimidazole and/or pyridine substitutions on the intrinsic affinity of the entering [Ln(hfa)$_3$] lanthanide containers (Scheme 2). Extension along the series monomer (**L3**) → dimer (**L6**) → trimer

(**L7**) takes into account the stepwise evolution from an isolated site in **L3**, toward two terminal sites in **L6** and finally to one central site flanked by two terminal sites in **L7**. From this set of original data, the transfer matrix formalism allows the safe prediction of the average intrinsic affinity of a single site in the polymer **P2**^{N} as a function of the total length *N*.

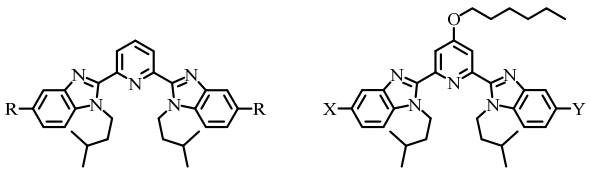

R = phenyl : **M1**
R = Br : **L1**
R = H : **L2**

X = Y = H : **L3**
X = Br; Y = H : **L4**
X = Y = Br : **L5**

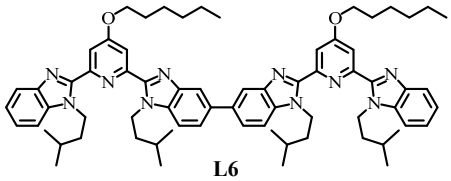

L6

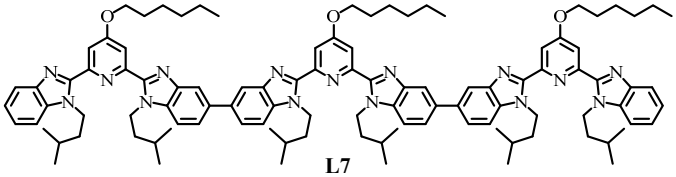

L7

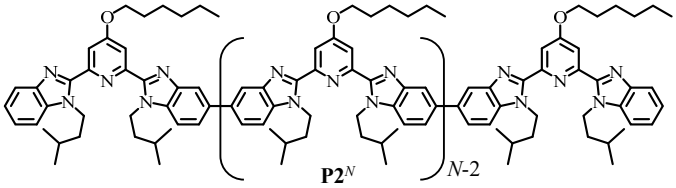

P2^{N} *N*-2

Scheme 2 Chemical structures of the segmental ligands used in this work.

Results and Discussion

Synthesis and molecular structures of ligands L3-L7 and of their saturated lanthanide adducts [L*k*Ln(hfa)$_3$] (L*k* = L3-L5), [L6(Ln(hfa)$_3$)$_2$] and [L7(Ln(hfa)$_3$)$_3$] (Ln = La, Eu, Yb, Lu). In order to be rid of the variable solvation effects produced by the original use of lipophilic dialkoxyphenyl bridges in the polymers **P1**^{N}, we have planned to design a novel polymeric backbone **P2**^{N}, in which the tridentate binding units are linked by direct $C_{aromatic}$-$C_{aromatic}$ bonds while hexyloxy chains bound to the pyridine rings and isopentyl chains bound to N-benzimidazole atoms ensure sufficient solubility in organic solvents. The model **L3**-**L5** monomers, dimer **L6** and trimer **L7** have been obtained

according to multistep strategies exploiting modified Philips reactions to form benzimidazole rings[22] as previously reported for preparing the reference ligands **M4**,[19a] **L1**[23] and **L2**[23] (Scheme S1 in the Supporting Information). Nickel-catalyzed homocoupling reactions provided reasonable yield (45%) of the symmetrical dimer **L6**,[24] whereas Suzuki-Miyaura cross-coupling reactions, despite considerable efforts for optimization, gave only poor yields (18%) of the trimer **L7** (Scheme 3 and Experimental section in the SI).[25]

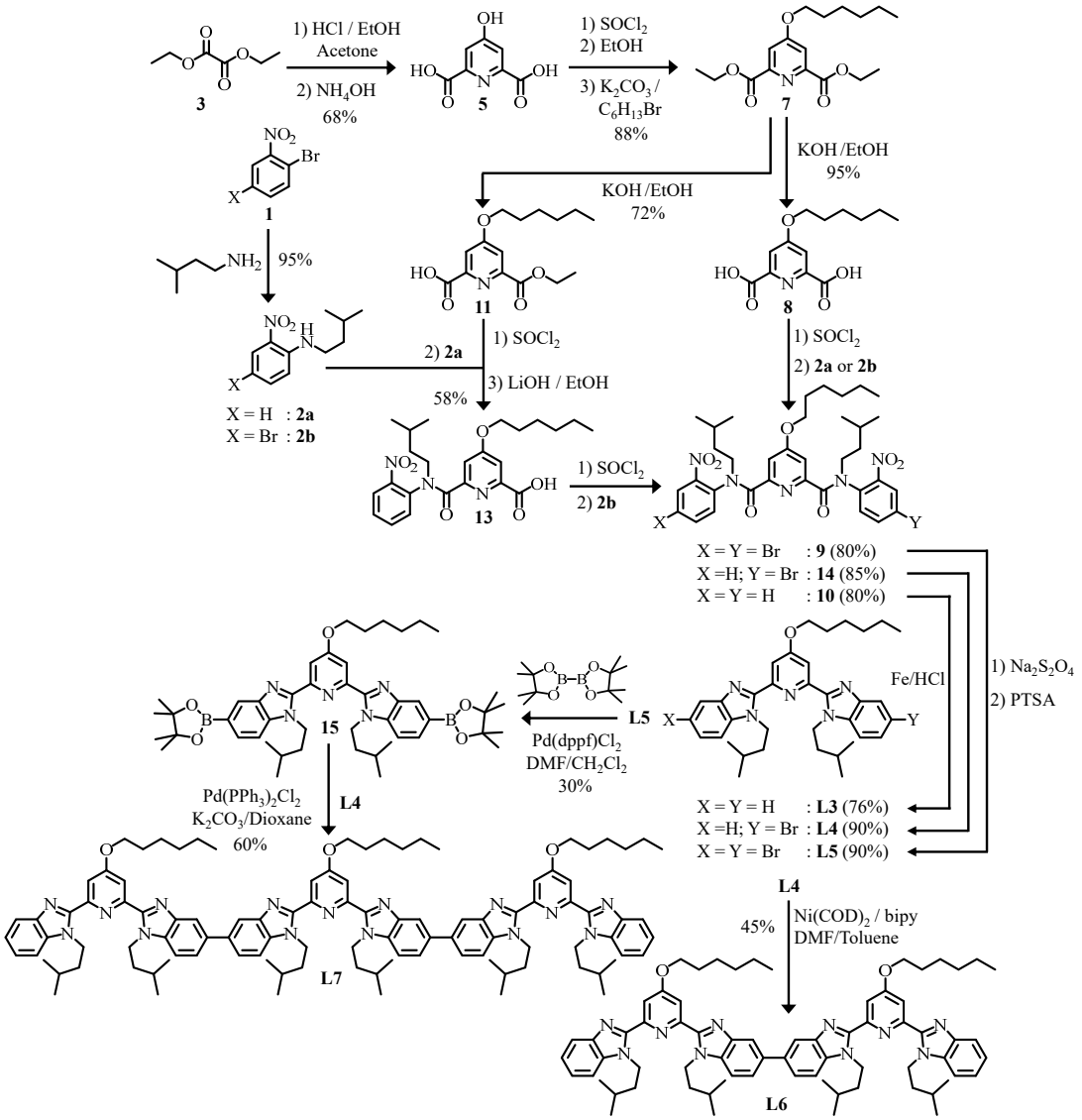

Scheme 3 Synthetic strategy used for the preparation of ligands **L3**-**L7**. PTSA = para-toluene sulfonic acid, bipy = 2,2' bipyridine, dpff = [1,1'-Bis(diphenylphosphino)ferrocene] and COD = 1,5-cyclooctadiene.

The ligands were characterized by ESI-MS (Experimental section in the SI) and elemental analysis (Table S1 in the SI). The ^{1}H NMR spectra of ligands **L3, L5, L6** and **L7** recorded in CD_2Cl_2 solutions show half the total number of aromatic protons together with enantiotopic signals for the methylene protons connected to the N-atom of the benzimidazole rings (Figure S1) in agreement with average planar C_{2v} symmetrical arrangements for these ligands on the NMR time scale. The absence of nuclear Overhauser effect between the two protons connected to the central pyridine ring and the protons of the isopentyl residues confirm that the three coordinating nitrogen atoms adopt the *transoid-transoid* geometry, which minimizes intramolecular electric dipole interactions in the free triimine ligands (illustrated in Scheme 3).[20] The non-symmetrical ligand **L4** displays the same structural characteristics in solution except for the lack of the twofold axis, which leads to only C_s symmetry on the NMR time scale and the doubling of the aromatic signals (Figure S1). Slow evaporation of methanol solutions for **L3**-**L5**, or of DMF solutions for **L6** produced X-ray quality prisms, the crystal structures of which are collected in Figure 3.

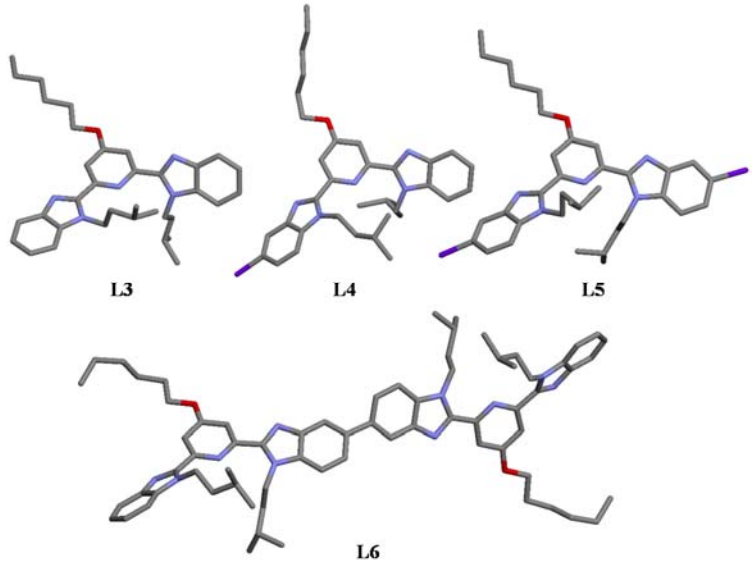

Figure 3. Views of the molecular structures of the ligands **L3-L6** as found in their crystal structures. Hydrogen atoms are omitted for clarity. Color code: C = grey, N = blue, O = red, Br = magenta.

All molecular structures confirm *transoid* conformations of the tridentate heterocyclic units (each non-substituted N atom of the benzimidazole ring adopts an *anti* conformation with respect to the nitrogen atom of the central pyridine ring to which it is connected). However, the benzimidazole(1)-

pyridine-benzimidazole(2) aromatic units are not coplanar due to the steric congestion imposed by the peripheral isopentyl groups, which leads to helical twists within the tridentate binding units as ascertained by pyridine-benzimidazole interplanar angles within the 3-55 degrees (Figures S2 and Tables S2-S8 in the Supporting Information). For the dimer **L6**, the two N atoms of the pyridine units are separated by 15.08 Å, which can be taken as a first rough estimate of the maximum intermetallic distance in the associated dinuclear complexes. The central biphenyl unit is twisted with a dihedral angle of about $\phi = 46°$, which is the result of a compromise between the repulsion of the hydrogen atoms connected at the ortho positions of the phenyl groups that are minimized by an orthogonal ($\phi = 90°$) arrangement, and the π-electron delocalization effect that is favored by a coplanar ($\phi = 0°$) organization.[26] Our efforts for crystallizing the trimeric ligand **L7** only failed, probably because of the larger number of degrees of freedom.

Reactions of stoichiometric amounts of **L3**-**L7** with [Ln(hfa)$_3$dig] (Ln = La, Eu, Lu; 1.0 eq. for **L3**-**L5**, 2.0 eq. for **L6** and 3.0 eq. for **L7**) in acetonitrile/dichloromethane (**L3**-**L5**) or acetonitrile/benzene (**L6**-**L7**) provided the complexes [**L*k***Ln(hfa)$_3$] (***k*** = 3-5), [**L6**(Ln(hfa)$_3$)$_2$] and [**L7**(Ln(hfa)$_3$)$_3$] with 50-90% yield (Table S1 in the Supporting Information). Slow evaporations of concentrated solutions gave single crystals of these complexes suitable for X-ray analysis (Figures 4a and S3, Figures S4-S7 and Tables S9-S40). For [**L7**(Eu(hfa)$_3$)$_3$], the best obtained crystals display only weak diffraction at high angle and the quality of the obtained model limits numerical analysis and comparison (See Table S35 and Figure S8 in the Supporting Information). For all [**L*k***Ln(hfa)$_3$] units, the central lanthanide cation is nine-coordinated by the three nitrogen donor atoms of a meridionally bound tridentate bis(benzimidazole)pyridine ligand (*cis*-*cis* conformation) and by six oxygen atoms of the three didentate hexafluoroacetylacetonate anions. The bound tridentate aromatic ligands are twisted and deviate from planarity (1.3° ≤ dihedral pyridine-benzimidazole angle ≤ 38.6°) in order to minimize steric congestion between the neopentyl groups and the hydrogen atoms of the pyridine ring (Tables S31-S33, S40).[23] The geometry of the [**L*k***Ln(hfa)$_3$] units were analyzed with the program Shape 2.1.[27] Among the possible arrangements for the nine-coordinated LnN_3O_6 units, the

lowest value of deviation was systematically found for a C_s-symmetrical geometry, in which a trigonal basal plane (N1, N4, O7) and a roughly parallel equatorial pentagonal plane (O2, O3, O5, O6, N2) defines a distorted muffin shape, which is capped by O4 (Figure 4 bottom and Table S11).

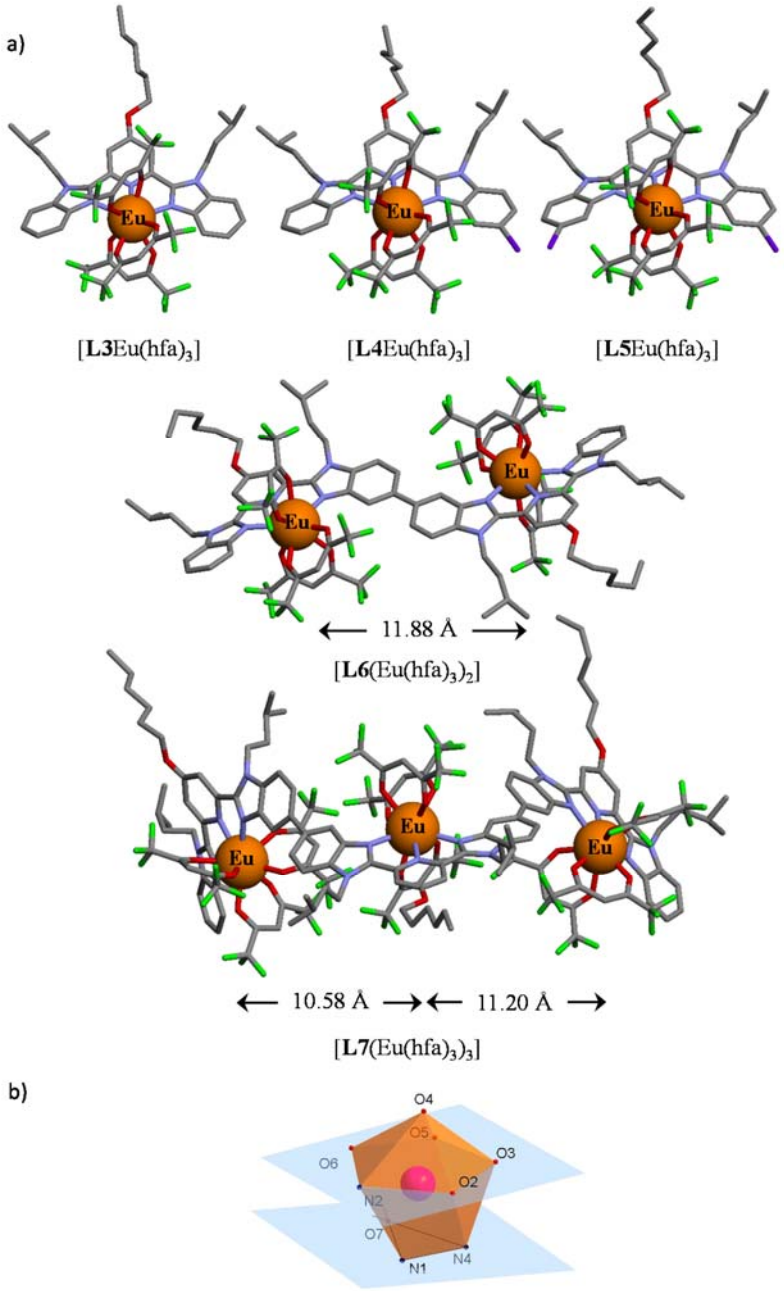

Figure 4. a) Views of the molecular structures of the complexes [**L*k***Eu(hfa)$_3$] (***k*** = 3-5), [**L6**(Eu(hfa)$_3$)$_2$] and [**L7**(Eu(hfa)$_3$)$_3$] as found in their crystal structures. Hydrogen atoms are omitted for clarity. Color code: C = grey, N = blue, O = red, F = light green, Br = magenta, Eu = orange. b) Muffin shape obtained by Shape analysis.[27]

Table 1 Average Bond Lengths (d), Bond Valences ($\bar{\nu}_{\text{Ln-N}}$ and $\bar{\nu}_{\text{Ln-O}}$) and Bond Valence Sums ($V_{\text{Ln},j}$) in the Crystal Structures of [**L*k***Eu(hfa)$_3$] (***k*** = 1-5), [**L6**(Eu(hfa)$_3$)$_2$] and [**L7**(Eu(hfa)$_3$)$_3$].

Complex	dLn-N(py) /Å	$\bar{\nu}_{\text{Ln-N(py)}}$ [a]	dLn-N(bzim) /Å [b]	$\bar{\nu}_{\text{Ln-N(bzim)}}$ [a,b]	$\bar{\nu}_{\text{Ln-N}}$ [a,b]	dLn-O(hfa) /Å [b]	$\bar{\nu}_{\text{Ln-O(hfac)}}$ [a,b]	$V_{\text{Ln},j}$ [b,c]	Reference
[**L1**Eu(hfa)$_3$]	2.613	0.295	2.57(3)	0.34(3)	0.32(3)	2.43(5)	0.35(4)	3.052	23
[**L2**Eu(hfa)$_3$]	2.570	0.331	2.540(1)	0.359(1)	0.35(2)	2.39(4)	0.39(4)	3.372	23
[**L3**Eu(hfa)$_3$]	2.627	0.284	2.529(2)	0.370(2)	0.34(5)	2.42(3)	0.36(3)	3.154	This work
[**L4**Eu(hfa)$_3$]	2.648	0.268	2.55(2)	0.35(2)	0.32(5)	2.42(3)	0.35(3)	3.086	This work
[**L5**Eu(hfa)$_3$]	2.627	0.284	2.562(3)	0.338(3)	0.32(3)	2.42(3)	0.36(2)	3.124	This work
[**L6**(Eu(hfa)$_3$)$_2$]	2.583	0.320	2.54(1)	0.36(1)	0.35(3)	2.43(3)	0.35(3)	3.143	This work
[**L7**(Eu(hfa)$_3$)$_3$] (terminal sites)	2.59(3)	0.31(2)	2.53(3)	0.37(3)	0.35(4)	2.41(4)	0.36(4)	3.24(6)	This work
[**L7**(Eu(hfa)$_3$)$_3$] (central site)	2.60	0.305	2.545(7)	0.354(7)	0.34(3)	2.43(4)	0.35(3)	3.131	This work

[a] $\nu_{\text{Ln},j} = \exp\left[\left(R_{\text{Ln},j} - d_{\text{Ln},j}\right)/b\right]$ where $d_{\text{Ln},j}$ is the bond length, $R_{\text{Ln},j}$ corresponds to the bond valence parameters and b = 0.37 Å is a universal scaling constant.[28b] Average of several values: the standard deviation of which is given between brackets. [c] $V_{\text{Ln}} = \sum_j \nu_{\text{Ln},j}$.

Upon the stepwise connection of electron-withdrawing bromine atoms to the peripheral benzimidazole rings along the [**L3**Eu(hfa)$_3$], [**L4**Eu(hfa)$_3$] and [**L5**Eu(hfa)$_3$] series, the Eu-N(pyridine) bond lengths is negligibly affected, (Table 1 column 2), but the Eu-N(benzimidazole) slightly increases (Table 1, column 4) as testified by related trends obtained for the associated bond valences $\bar{\nu}_{\text{Ln-N(py)}}$ and $\bar{\nu}_{\text{Ln-N(bzim)}}$, which can be considered as quantitative measures of the strength of the ligand-metal interactions (Table 1, columns 3 and 5).[28] This indicates that the electronic density on the nitrogen atoms of the imidazole N-donor atom can be modulated by substitution of the fused phenyl ring at the 5 position. Surprisingly, the connection of a hexyloxy group at the 4-position of the central pyridine ring which transforms [**L2**Eu(hfa)$_3$] into [**L3**Eu(hfa)$_3$] or [**L1**Eu(hfa)$_3$] into [**L5**Eu(hfa)$_3$] results in an unexpected increase of the Eu-N(pyridine) bond lengths and weaker metal-ligand interactions although alkoxy groups are considered as donors groups in organic chemistry (Hammett coefficient σ_{para} = -0.28).[29] In line with previous observations with **M1**, **L1** and **L2**, the average bond valences computed for [**L3**Eu(hfa)$_3$] along the lanthanide series confirms the maximum ligand-metal interactions occurring for the middle of the series ($\bar{\nu}_{\text{La-N}} \leq \bar{\nu}_{\text{Eu-N}} > \bar{\nu}_{\text{Lu-N}}$, Tables 1 and S41) and therefore a preference for complexing mid-range lanthanides in these adducts.[20,23] Finally, in term of average bond valences, the negatively charged oxygen donors of the electron-withdrawing hexafluoroacetylacetonate co-ligands provide Ln-O interactions, the strengths of which are comparable with those found for bound heterocyclic nitrogen atoms (Table 1, column 8). Focusing on molecular structures, one observes that the stepwise shrinking of the Ln-ligand bond along the lanthanide series regularly increases the chelate binding angles (Table S12), whereas significant torsion angles between the aromatic planes of the tridentate ligand optimize its wrapping around the metallic center (Tables S20-S21).[23] The same trends can be observed in the dinuclear [**L6(**Ln(hfa)$_3$)$_2$] complexes (Ln = La, Eu, Yb, Lu Tables S22-S26 and S41) together with the additional consideration of (i) intramolecular intermetallic separations in the range of 10.5-11.9 Å (Figure 4 and S3, Table S42) and biphenyl dihedral angles of 0° for the centrosymmetrical [**L6(**Ln(hfa)$_3$)$_2$] (Ln = La, Eu) and

43-46° for Ln = Yb, Lu (Table S42). The limited quality of the crystal structures of [**L7(**Eu(hfa)$_3$)$_3$] prevents similar analysis with this complex, but the low-resolution picture confirms very similar structural characteristics.

In dichloromethane solution, the ^{1}H NMR spectrum of [**L3**Ln(hfa)$_3$] shows one set of signals for the two benzimidazole side arms (Figure S10) and the ^{19}F NMR trace displays a singlet for the six CF_3 groups of the three didentate hexafluoroacetylacetonate anions. These observations cannot be reconciled with the approximate C_s symmetry point group found in the solid state (Figures 4 and S3). We deduce that fast dynamic processes occur on the NMR time scale, which interconvert the bound axial and equatorial didentate hfa$^-$ co-ligands and make these chelating anions equivalent. Altogether, the coordinated tridentate ligand **L3** adopts a symmetry-averaged C_{2V} arrangement on the NMR time scale and the hfa$^-$ anions are related by dynamic re-organization around a threefold axis.[30] Related dynamic processes control the solution structures of the dimers [**L6**(Ln(hfa)$_3$)$_2$] (Figure S11) and trimers [**L7**(Ln(hfa)$_3$)$_3$] (Figure S12), in which the bound multi-tridentate ligands exhibit average C_{2V} symmetry compatible with two identical terminal nine-coordinate sites in [**L6**(Ln(hfa)$_3$)$_2$], and one different central and two identical terminal sites in [**L7**(Ln(hfa)$_3$)$_3$]. As expected, the complexation of **L*k*** to paramagnetic Eu(III) induces large downfield ^{1}H NMR shifts for the benzimidazole protons that are located close to the paramagnetic metallic center (H2 in [**L3**Eu(hfa)$_3$], Figure S10; H3 and H6 in [**L6**(Eu(hfa)$_3$)$_2$], Figure S11; H14, H17 and H20 in [**L7**(Eu(hfa)$_3$)$_3$], Figure S12).[21] Combined with the nuclear Overhauser enhancement effects (NOE) detected between the protons of the isopentyl residues and those of the attached pyridine ring, one can deduce that the tridendate units are meridionally bound to the central lanthanide cation (*cis-cis* conformation). Finally, additional NOE effects recorded between some specific pairs of protons in the biphenyl connectors (H17···H18 in [**L6**(Ln(hfa)$_3$)$_2$], and H17···H21 and H18···H20 in [**L7**(Ln(hfa)$_3$)$_3$]) evidence a dynamically-average *opposite* arrangements of the two successive coordination units in the polynuclear complexes as depicted in the solid state (Figure 4).

Thermodynamic formation of [L*k*Ln(hfa)$_3$] (L*k* = L3-L5), [L6(Ln(hfa)$_3$)$_m$] (*m* = 1, 2) and [L7(Ln(hfa)$_3$)$_m$] (*m* = 1-3) with Ln = La, Eu, Lu in dichloromethane.

The structural characterization of ligands **L3**, **L6** and **L7** and of their adducts [**L3**Ln(hfa)$_3$], [**L6**(Ln(hfa)$_3$)$_2$] and [**L7**(Ln(hfa)$_3$)$_3$] in the solid state and in solution suggests that the complexation processes operating in solution can be summarized by the exchange equilibria (4)-(6).

$$\mathbf{L3} + [\mathrm{Ln(hfa)_3dig}] \rightleftharpoons [\mathbf{L3}\mathrm{Ln(hfa)_3}] + \mathrm{dig} \qquad \beta_{1,1,\mathrm{exch}}^{\mathrm{Ln},\mathbf{L3}} \qquad (4)$$

$$\mathbf{L6} + m\,[\mathrm{Ln(hfa)_3dig}] \rightleftharpoons [\mathbf{L6}(\mathrm{Ln(hfa)_3})_m] + m\,\mathrm{dig} \qquad \beta_{m,1,\mathrm{exch}}^{\mathrm{Ln},\mathbf{L6}}\ (m=1,2) \qquad (5)$$

$$\mathbf{L7} + m\,[\mathrm{Ln(hfa)_3dig}] \rightleftharpoons [\mathbf{L7}(\mathrm{Ln(hfa)_3})_m] + m\,\mathrm{dig} \qquad \beta_{m,1,\mathrm{exch}}^{\mathrm{Ln},\mathbf{L7}}\ (m=1\text{-}3) \qquad (6)$$

Previous ^{1}H NMR studies of [**M1**Ln(hfa)$_3$],[19] [**L1**Ln(hfa)$_3$] and [**L2**Ln(hfa)$_3$][23] complexes in dichloromethane have established the formation of these complexes at submillimolar concentrations with no detectable dissociation of the hfa counter-anions and for wide range of occupancy factors ($0.05 \le \theta_{\mathrm{Ln}} \le 0.95$ with $\theta_{\mathrm{Ln}} = [\mathrm{Ln}]_{\mathrm{bound}} / [\mathbf{L}]_{\mathrm{tot}}$). For the sake of simplicity, the concentrations of complex species [L*k*Ln(hfa)$_3$] and [Ln(hfa)$_3$dig] will be written as $|\mathbf{L}k\mathrm{Ln}|$ and $|\mathrm{Lndig}|$ respectively, for the rest of this contribution. Taking equilibrium (4) as a working example, classical thermodynamics associates a free energy change $\Delta G_{1,1,\mathrm{exch}}^{\mathrm{Ln},\mathbf{L3}}$ and a stability constant $\beta_{1,1,\mathrm{exch}}^{\mathrm{Ln},\mathbf{L3}}$ summarized in eqn (7), where $a_i = \gamma_i (c_i / c^{\theta})$ are the activities, γ_i are the activity coefficients, c^{θ} is the standard concentration of the reference state arbitrarily fixed at 1.0 M and $Q_{1,1,\mathrm{exch}}^{\mathrm{Ln},\mathbf{L3}}$ is the equilibrium quotient of the reaction.

$$\beta_{1,1,\mathrm{exch}}^{\mathrm{Ln},\mathbf{L3}} = \exp\left(-\frac{\Delta G_{1,1,\mathrm{exch}}^{\mathrm{Ln},\mathbf{L3}}}{RT}\right) = \frac{a_{\mathbf{L3}\mathrm{Ln}}^{\mathrm{eq}} \cdot a_{\mathrm{dig}}^{\mathrm{eq}}}{a_{\mathrm{Lndig}}^{\mathrm{eq}} \cdot a_{\mathbf{L3}}^{\mathrm{eq}}} = \frac{\gamma_{\mathbf{L3}\mathrm{Ln}}\left(|\mathbf{L3}\mathrm{Ln}|_{\mathrm{eq}} / c^{\theta}\right) \cdot \gamma_{\mathrm{dig}}\left(|\mathrm{dig}|_{\mathrm{eq}} / c^{\theta}\right)}{\gamma_{\mathrm{Lndig}}\left(|\mathrm{Lndig}|_{\mathrm{eq}} / c^{\theta}\right) \cdot \gamma_{\mathbf{L3}}\left(|\mathbf{L3}|_{\mathrm{eq}} / c^{\theta}\right)}$$

$$\Rightarrow \beta_{1,1,\mathrm{exch}}^{\mathrm{Ln},\mathbf{L3}} = \frac{\gamma_{\mathbf{L3}\mathrm{Ln}}\gamma_{\mathrm{dig}}}{\gamma_{\mathrm{Lndig}}\gamma_{\mathbf{L3}}} \cdot \frac{|\mathbf{L3}\mathrm{Ln}|_{\mathrm{eq}}\,|\mathrm{dig}|_{\mathrm{eq}}}{|\mathrm{Lndig}|_{\mathrm{eq}}\,|\mathbf{L3}|_{\mathrm{eq}}} = \frac{\gamma_{\mathbf{L3}\mathrm{Ln}}\gamma_{\mathrm{dig}}}{\gamma_{\mathrm{Lndig}}\gamma_{\mathbf{L3}}} \cdot Q_{1,1,\mathrm{exch}}^{\mathrm{Ln},\mathbf{L3}} \qquad (7)$$

In aqueous solution, the theory of the ionic atmosphere (Debye-Hückel) allows to fix the activity coefficients γ_i whatever the composition of the solution thanks to the use of a large excess of non-

coordinating electrolytes. The thermodynamic constant $\beta_{1,1,\text{exch}}^{\text{Ln},\mathbf{L3}}$ is then proportional to the experimental quotient of reaction $Q_{1,1,\text{exch}}^{\text{Ln},\mathbf{L3}}$ for any mixtures under thermodynamic equilibrium. The situation becomes more 'tricky' for equilibria studied in organic solvents in absence of fixed ionic strength such as those considered here where a multidentate chelate ligand **L*k*** displaces a diglyme molecule from [Ln(hfa)$_3$dig] in dichloromethane solution to give [**L*k***Ln(hfa)$_3$] (eqn 4).[31] In these conditions, the Margules equations[32] predict that the activity coefficients γ_i are sensitive to the concentrations of the dissolved species and $Q_{1,1,\text{exch}}^{\text{Ln},\mathbf{L3}}$ is no more constant during a host-guest titration process.[21] An intuitive and simple balance of chemical potentials pertinent to host-guest association equilibria led Eggers and co-workers to propose eqn (8),[33] which catches the variation of the activity coefficients with the progress of the reaction measured by the equilibrium concentration $\left|\mathbf{L3}\text{Ln}\right|_{\text{eq}}$ of the final [**L3**Ln(hfa)$_3$] complex. The ordinate of the linear plot of $-RT\ln\left(Q_{1,1,\text{exch}}^{\text{Ln},\mathbf{L3}}\right)$ as a function of $\left|\mathbf{L3}\text{Ln}\right|_{\text{eq}}$ corresponds to a reliable thermodynamic free energy change $\Delta G_{1,1,\text{exch}}^{\text{Ln},\mathbf{L3},\infty}$ at infinite dilution, while the slope (i.e. the factor of proportionality) is written as a free-energy change $\Delta G_{1,1,\text{exch}}^{\text{Ln},\mathbf{L3},\text{S}}$ assigned to some solvation effects accompanying the association reaction, which are not taken into account by the standard chemical potentials of the various species at equilibrium.[21,31,33]

$$-RT\ln\left(Q_{1,1,\text{exch}}^{\text{Ln},\mathbf{L3}}\right)=\Delta G_{1,1,\text{exch}}^{\text{Ln},\mathbf{L3},\infty}+\left(\left|\mathbf{L3}\text{Ln}\right|_{\text{eq}}/c^{\theta}\right)\Delta G_{1,1,\text{exch}}^{\text{Ln},\mathbf{L3},\text{S}} \qquad (8)$$

In practice, the ^{1}H NMR monitoring of the titration of 0.7 mL of a 10 mM solution of ligand **L3** with a concentrated solution (100 mM) of [Ln(hfa)$_3$dig] (Ln = La, Eu, Lu) in pure dichloromethane unambiguously demonstrates the stepwise formation of [**L3**Ln(hfa)$_3$] as the single product complex according to equilibrium (4) (Figure 5). In addition, for each step of the titration, the ^{1}H NMR spectra recorded at thermodynamic equilibrium do not show any dynamic exchange process on the NMR time scale. In these conditions, and for the sake of simplicity, we consider that all considered concentrations correspond to equilibrium concentrations and the 'eq' term is removed for the rest of the discussion.

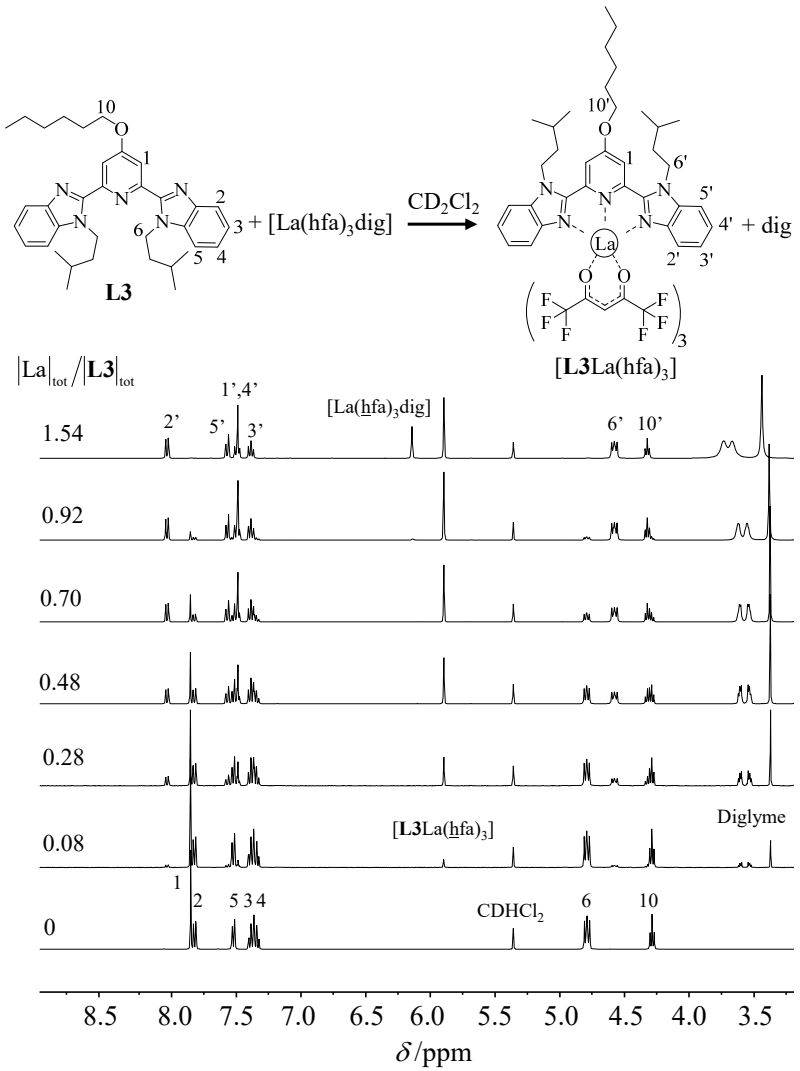

Figure 5. ^{1}H NMR titration of **L3** (29 mM**)** with [La(hfa)3dig] in pure CD_2Cl_2 at 293 K.

Accordingly, the integrated ^{1}H NMR signals can be safely taken as quantitative estimations of the free ($I^{\mathrm{H}}_{\mathbf{L3}}$) and complexed ($I^{\mathrm{H}}_{\mathbf{L3}\mathrm{Ln}}$) ligand for each mixture of ligand and metal, from which the occupancy factors $\theta^{\mathbf{L3},\mathrm{exp}}_{\mathrm{Ln}}$ and the free concentration of metal $\left|\mathrm{Lndig}\right| = \left|\mathbf{Ln}\right|_{\mathrm{tot}} - \theta^{\mathbf{L3},\mathrm{exp}}_{\mathrm{Ln}} \left|\mathbf{L3}\right|_{\mathrm{tot}}$ can be computed (eqn 9).

$$\theta^{\mathbf{L}k,\mathrm{exp}}_{\mathrm{Ln}} = \frac{\left|\mathrm{Ln}\right|_{\mathrm{bound}}}{\left|\mathbf{L3}\right|_{\mathrm{tot}}} = \frac{\left|\mathbf{L3}\mathrm{Ln}\right|_{\mathrm{bound}}}{\left|\mathbf{L3}\right|_{\mathrm{tot}}} = \frac{I^{\mathrm{H}}_{\mathbf{L3}\mathrm{Ln}}}{I^{\mathrm{H}}_{\mathbf{L3}} + I^{\mathrm{H}}_{\mathbf{L3}\mathrm{Ln}}} = \frac{\left|\mathrm{Ln}\right|_{\mathrm{tot}} - \left|\mathrm{Lndig}\right|}{\left|\mathbf{L3}\right|_{\mathrm{tot}}} \tag{9}$$

Application of the mass balance provides the missing concentrations of $\left|\mathrm{dig}\right| = \left|\mathbf{L3}\mathrm{Ln}\right| = \theta^{\mathbf{L3},\mathrm{exp}}_{\mathrm{Ln}} \left|\mathbf{L3}\right|_{\mathrm{tot}}$ and $\left|\mathbf{L3}\right| = \left|\mathbf{L3}\right|_{\mathrm{tot}} \left(1 - \theta^{\mathbf{L3},\mathrm{exp}}_{\mathrm{Ln}}\right)$, from which the equilibrium quotients of reaction $Q^{\mathrm{Ln},\mathbf{L3}}_{1,1,\mathrm{exch}}$ can be

calculated (eqn 7). Plot of $-RT\ln\left(Q_{1,1,\text{exch}}^{\text{Ln},\mathbf{L3}}\right)$ with respect to the advance of the titration processes measured with $|\mathbf{L3}\text{Ln}|$ indeed display satisfying straight lines (Figures 6a and S13a, left part) in agreement with eqn (8), from which (i) the thermodynamic free energies $\Delta G_{1,1,\text{exch}}^{\text{Ln},\mathbf{L3},\infty}$ and $\Delta G_{1,1,\text{exch}}^{\text{Ln},\mathbf{L3},\text{S}}$ can be deduced (Table 2) together with (ii) the associated pseudo-binding isotherms (eqn 10, Figure 6b and S13b; left part).[21]

$$\theta_{\text{Ln}}^{\mathbf{L3},\text{calc}} = \frac{|\mathbf{L3}\text{Ln}|}{|\mathbf{L3}|_{\text{tot}}} = \frac{Q_{1,1,\text{exch}}^{\text{Ln},\mathbf{L3}}\,|\text{Lndig}|/|\text{dig}|}{1+Q_{1,1,\text{exch}}^{\text{Ln},\mathbf{L3}}\,|\text{Lndig}|/|\text{dig}|} \qquad (10)$$

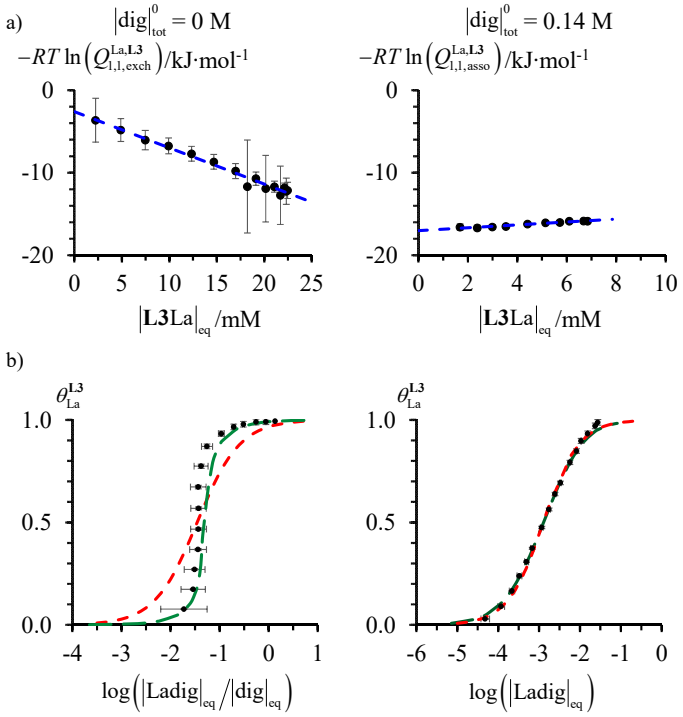

Figure 6. a) Dependences of the equilibrium quotients $Q_{1,1,\text{exch}}^{\text{La},\mathbf{L3}}$ ($|\text{dig}|_{\text{tot}}^{0}$ = 0 M, left part) and $Q_{1,1,\text{asso}}^{\text{La},\mathbf{L3}}$ ($|\text{dig}|_{\text{tot}}^{0}$ = 0.14 M, right part) on the progress of the titration of **L3** with [La(hfac)$_3$dig] (eqn 8) and b) associated binding isotherms (black dots). The green traces correspond to the fits obtained with eqn (11) and variable activity coefficients, whereas the red traces are fitted with eqn (14) and constant activity coefficients.

With these free energies in mind, the introduction of eqn (8) into eqn (10) gives eqn (11), from which the occupancy factors can be computed for any point along the titration as soon as $|\mathbf{L3}|_{\text{tot}}$ and $|\text{Ln}|_{\text{tot}}$ have been fixed (dashed green traces in Figures 6b and S13b; left part).

$$\theta_{\mathrm{Ln}}^{\mathbf{L3},\mathrm{calc}} = \frac{\left|\mathbf{L3}\mathrm{Ln}\right|}{\left|\mathbf{L3}\right|_{\mathrm{tot}}} = \frac{\exp\left\{-\left[\Delta G_{1,1,\mathrm{exch}}^{\mathrm{Ln},\mathbf{L3},\infty} + \left(\left|\mathbf{L3}\mathrm{Ln}\right|/c^{\theta}\right)\Delta G_{1,1,\mathrm{exch}}^{\mathrm{Ln},\mathbf{L3},\mathrm{S}}\right]/RT\right\}\left[\left(\left|\mathrm{Ln}\right|_{\mathrm{tot}} - \left|\mathbf{L3}\mathrm{Ln}\right|\right)/\left|\mathbf{L3}\mathrm{Ln}\right|\right]}{1+\exp\left\{-\left[\Delta G_{1,1,\mathrm{exch}}^{\mathrm{Ln},\mathbf{L3},\infty} + \left(\left|\mathbf{L3}\mathrm{Ln}\right|/c^{\theta}\right)\Delta G_{1,1,\mathrm{exch}}^{\mathrm{Ln},\mathbf{L3},\mathrm{S}}\right]/RT\right\}\left[\left(\left|\mathrm{Ln}\right|_{\mathrm{tot}} - \left|\mathbf{L3}\mathrm{Ln}\right|\right)/\left|\mathbf{L3}\mathrm{Ln}\right|\right]} \quad (11)$$

The variation of the equilibrium quotients of the reaction $Q_{1,1,\mathrm{exch}}^{\mathrm{Ln},\mathbf{L3}}$ during the titration process in CD_2Cl_2, which is assigned to change in activity coefficients[21] and/or to uncompensated solvation effects,[33] are indeed considerable ($\Delta G_{1,1,\mathrm{exch}}^{\mathrm{La},\mathbf{L3},\mathrm{S}}$ = -438(18) kJ·mol^{-1} and $\Delta G_{1,1,\mathrm{exch}}^{\mathrm{Eu},\mathbf{L3},\mathrm{S}}$ = -2360(193) kJ·mol^{-1}, column 4, entries 2-3 in Table 2). The associated corrections at 10 mM concentration amount to 5 $\leq \left(\left|\mathbf{L3}\mathrm{Ln}\right|_{\mathrm{eq}}/c^{\theta}\right)\Delta G_{1,1,\mathrm{asso}}^{\mathrm{Ln},\mathbf{L3},\mathrm{S}} \leq$ 25 kJ·mol^{-1} and dominate the host-guest association processes ($\Delta G_{1,1,\mathrm{exch}}^{\mathrm{La},\mathbf{L3},\infty}$ = -2.7(3) kJ·mol^{-1} and $\Delta G_{1,1,\mathrm{exch}}^{\mathrm{La},\mathbf{L3},\infty}$ = 4.1(1) kJ·mol^{-1}, column 3 in Table 2). In these conditions, comparing affinity between different systems is elusive and not realistic in pure dichloromethane.

Table 2. Thermodynamic Parameters $\Delta G_{1,1,\mathrm{exch}}^{\mathrm{Ln},\mathbf{L3},\infty}$ and $\Delta G_{1,1,\mathrm{exch}}^{\mathrm{Ln},\mathbf{L3},\mathrm{S}}$ (eqn 8) and $\Delta G_{1,1,\mathrm{asso}}^{\mathrm{Ln},\mathbf{L3}} = -RT\ln\left(\beta_{1,1,\mathrm{asso}}^{\mathrm{Ln},\mathbf{L3}}\right)$ (eqn 12) Calculated for the Titrations of **L3** (10 mM) with [Ln(hfa)$_3$dig] (Ln = Eu, La) in CD_2Cl_2 with $\left|\mathrm{dig}\right|_{\mathrm{tot}}^{0}$ = 0, 0.14, 0.45 and 0.94 M at 293 K

Ln	$\left\|\mathrm{dig}\right\|_{\mathrm{tot}}^{0}$ /M	$\Delta G_{1,1,\mathrm{exch}}^{\mathrm{Ln},\mathbf{L3},\infty}$ / kJ·mol^{-1}	$\Delta G_{1,1,\mathrm{exch}}^{\mathrm{Ln},\mathbf{L3},\mathrm{S}}$ / kJ·mol^{-1}	$\Delta G_{1,1,\mathrm{asso}}^{\mathrm{Ln},\mathbf{L3}}$ / kJ·mol^{-1}	$\beta_{1,1,\mathrm{asso}}^{\mathrm{Ln},\mathbf{L3}}$	$\beta_{1,1,\mathrm{exch}}^{\mathrm{Ln},\mathbf{L3}}$ [a]
La	0	-2.7(3)	-438(18)	-	-	-
Eu	0	4.1(1)	-2360(193)	-	-	-
La	0.14	-17.1(4) [b]	176(15) [b]	-16.3(1)	789(26)	120(4)
Eu	0.14	-21.2(7) [b]	212(100) [b]	-20.4(3)	4200(407)	593(58)
La	0.45	-13.1(2) [b]	-262(38) [b]	-13.9(1)	312(12)	143(6)
Eu	0.45	-14.8(5) [b]	-407(70) [b]	-17.1(2)	1084(82)	514(39)
La	0.94	-10.7(2) [b]	-83(33) [b]	-10.9(1)	88(2)	83(2)
Eu	0.94	-13.5(3) [b]	-294(42) [b]	-15.2(2)	505(42)	475(39)

[a] $\beta_{1,1,\mathrm{exch}}^{\mathrm{Ln},\mathbf{L3}} = \beta_{1,1,\mathrm{asso}}^{\mathrm{Ln},\mathbf{L3}}\left|\mathrm{dig}\right|_{\mathrm{tot}}$. [b] For $\left|\mathrm{dig}\right|_{\mathrm{tot}}^{0} \neq 0$, $\Delta G_{1,1,\mathrm{asso}}^{\mathrm{Ln},\mathbf{L3},\infty}$ and $\Delta G_{1,1,\mathrm{asso}}^{\mathrm{Ln},\mathbf{L3},\mathrm{S}}$ are computed by using $-RT\ln\left(Q_{1,1,\mathrm{asso}}^{\mathrm{Ln},\mathbf{L3}}\right) = \Delta G_{1,1,\mathrm{asso}}^{\mathrm{Ln},\mathbf{L3},\infty} + \left(\left|\mathbf{L3}\mathrm{Ln}\right|_{\mathrm{eq}}/c^{\theta}\right)\Delta G_{1,1,\mathrm{asso}}^{\mathrm{Ln},\mathbf{L3},\mathrm{S}}$ and reported here (see Figure 6a right).

However, as suggested by the Margules equations,[21] the situation simplifies when at least one reactant or product can be set at a fixed concentration, and in large excess with respect to the other components

involved in the chemical equilibrium. By introducing an initial concentration of diglyme in large excess, so that $|\mathrm{dig}| \cong |\mathrm{dig}|_{\mathrm{tot}}^{0}$ along the complete titration process, the equilibrium quotient of the exchange reaction $Q_{1,1,\mathrm{exch}}^{\mathrm{Ln},\mathbf{L3}}$ transforms into $Q_{1,1,\mathrm{asso}}^{\mathrm{Ln},\mathbf{L3}} = Q_{1,1,\mathrm{exch}}^{\mathrm{Ln},\mathbf{L3}} / |\mathrm{dig}|_{\mathrm{tot}}$ (eqn 12), which corresponds to the simple host-guest equilibrium (13) characterized by a conditional stability constants $\beta_{1,1,\mathrm{asso}}^{\mathrm{Ln},\mathbf{L3}}$, the values of which depends on $|\mathrm{dig}|_{\mathrm{tot}}^{0}$.[21]

$$Q_{1,1,\mathrm{asso}}^{\mathrm{Ln},\mathbf{L3}} = \frac{Q_{1,1,\mathrm{exch}}^{\mathrm{Ln},\mathbf{L3}}}{|\mathrm{dig}|_{\mathrm{tot}}} = \frac{|\mathbf{L3}\mathrm{Ln}|_{\mathrm{eq}}}{|\mathrm{Lndig}|_{\mathrm{eq}} |\mathbf{L3}|_{\mathrm{eq}}} = \frac{\gamma_{\mathrm{Lndig}}\gamma_{\mathbf{L3}}}{\gamma_{\mathbf{L3}\mathrm{Ln}}\gamma_{\mathrm{dig}}} \frac{\beta_{1,1,\mathrm{exch}}^{\mathrm{Ln},\mathbf{L3}}}{|\mathrm{dig}|_{\mathrm{tot}}} = \frac{\gamma_{\mathrm{Lndig}}\gamma_{\mathbf{L3}}}{\gamma_{\mathbf{L3}\mathrm{Ln}}\gamma_{\mathrm{dig}}} \beta_{1,1,\mathrm{asso}}^{\mathrm{Ln},\mathbf{L3}} \qquad (12)$$

$$\mathbf{L3} \quad + \quad [\mathrm{Ln(hfa)_3}] \quad \rightleftharpoons \quad [\mathbf{L3}\mathrm{Ln(hfa)_3}] \qquad \beta_{1,1,\mathrm{asso}}^{\mathrm{Ln},\mathbf{L3}} = \beta_{1,1,\mathrm{exch}}^{\mathrm{Ln},\mathbf{L3}} / |\mathrm{dig}|_{\mathrm{tot}} \qquad (13)$$

As expected,[21] titrations of **L3** with [Ln(hfa)$_3$dig] performed in dichloromethane containing an excess of diglyme ($|\mathrm{dig}|_{\mathrm{tot}}^{0} \geq 0.1$ M, Figure S14) limit the variation of the activity coefficients and the equilibrium quotients $Q_{1,1,\mathrm{asso}}^{\mathrm{Ln},\mathbf{L3}} = |\mathbf{L3}\mathrm{Ln}|_{\mathrm{eq}} / \left(|\mathrm{Lndig}|_{\mathrm{eq}} |\mathbf{L3}|_{\mathrm{eq}} \right)$ of the association reaction (eqn 12) are roughly constant (right parts of Figure 6a and S13a and Figure S15), which implies that the activity coefficients only loosely vary during the titration process conducted in these conditions (eqn 12). It is therefore safe to consider $Q_{1,1,\mathrm{asso}}^{\mathrm{Ln},\mathbf{L3}}$ as a reliable estimation of the thermodynamic conditional affinity constant $\beta_{1,1,\mathrm{asso}}^{\mathrm{Ln},\mathbf{L3}}$. The binding isotherm can be now built by using the classical Langmuir formula given in eqn (14) for a 1:1 host-guest association process.

$$\theta_{\mathrm{Ln}}^{\mathbf{L3},\mathrm{calc}} = \frac{|\mathbf{L3}\mathrm{Ln}|}{|\mathbf{L3}|_{\mathrm{tot}}} = \frac{\beta_{1,1,\mathrm{asso}}^{\mathrm{Ln},\mathbf{L3}} |\mathrm{Lndig}|}{1 + \beta_{1,1,\mathrm{asso}}^{\mathrm{Ln},\mathbf{L3}} |\mathrm{Lndig}|} \qquad (14)$$

The best fits of the experimental data using eqn (14) are depicted as red traces in Figures 6b, S14b and S15. As long as $|\mathrm{dig}|_{\mathrm{tot}}^{0} \geq 0.1$ M, the two methods converge and the associated conditional stability constants $\beta_{1,1,\mathrm{asso}}^{\mathrm{Ln},\mathbf{L3}}$ (Table 2, column 6) can be used for the estimation of the exchange constants $\beta_{1,1,\mathrm{exch}}^{\mathrm{Ln},\mathbf{L3}} = \beta_{1,1,\mathrm{asso}}^{\mathrm{Ln},\mathbf{L3}} |\mathrm{dig}|_{\mathrm{tot}}$ in the solvent of interest (Table 2 column 7).

The latter method could be satisfyingly applied for the titrations of **L3**-**L5** with [Ln(hfac)$_3$dig] in CD_2Cl_2 + $\left|\mathrm{dig}\right|_{\mathrm{tot}}^{0}$ = 0.14 M, where the experimental occupancy factors deduced from integration of the ^{1}H NMR data are fitted to the theoretical Langmuir isotherms (eqn 14) to give the conditional stability constants $\beta_{1,1,\mathrm{asso}}^{\mathrm{Ln},\mathbf{Lk}}$ gathered in Table 3 (entry 3). Similarly, titrations of dimer **L6** (Figures S16-S18) and trimer **L7** (Figures S19-S21) monitored by ^{1}H and ^{19}F- NMR with [Ln(hfac)$_3$dig] in CD_2Cl_2 + $\left|\mathrm{dig}\right|_{\mathrm{tot}}^{0}$ = 0.14 M provide the experimental occupancy factors $\theta_{\mathrm{Ln}}^{\mathbf{Lk},\mathrm{exp}}$ by integration of the NMR signals. Fitting to the extended binding isotherm eqn (15) finally gives the conditional stability constants $\beta_{m,1,\mathrm{asso}}^{\mathrm{Ln},\mathbf{Lk}}$ collected in Table 4 (**L6** with m = 1-2 and N = 2 and **L7** with m = 1-3 and N = 3)

$$\theta_{\mathrm{Ln}}^{\mathbf{Lk},\mathrm{calc}} = \frac{\left|\mathrm{Ln}\right|_{\mathrm{bound}}}{N\left|\mathbf{Lk}\right|_{\mathrm{tot}}} = \frac{\sum_{m=1}^{N}\left|\mathbf{Lk}\mathrm{Ln}_m\right|}{N\left|\mathbf{Lk}\right|_{\mathrm{tot}}} = \frac{\sum_{m=1}^{N} m\beta_{m,1,\mathrm{asso}}^{\mathrm{Ln},\mathbf{L3}}\left|\mathrm{Lndig}\right|^m}{1+\sum_{m=1}^{N}\beta_{m,1,\mathrm{asso}}^{\mathrm{Ln},\mathbf{L3}}\left|\mathrm{Lndig}\right|^m} \qquad (15)$$

The conditional stability constants $\beta_{1,1,\mathrm{asso}}^{\mathrm{Ln},\mathbf{Lk}}$ measured for the monomers **M1**, **L1**-**L5** (Table 3) demonstrate three striking trends. Firstly, the connection of alkoxy groups at the 4-position (para) of the central pyridine rings increases the host-guest affinity by a factor 2-3 as illustrated by $\beta_{1,1,\mathrm{asso}}^{\mathrm{La},\mathbf{L1}}$ = 55(3) which is transformed into $\beta_{1,1,\mathrm{asso}}^{\mathrm{La},\mathbf{L5}}$ = 116(4) and by $\beta_{1,1,\mathrm{asso}}^{\mathrm{La},\mathbf{L2}}$ = 265(20) which increases to reach $\beta_{1,1,\mathrm{asso}}^{\mathrm{La},\mathbf{L3}}$ = 789(26). This trend contrasts with Eu-N(pyridine) bond lengths measured in the solid state and highlights the gap between thermodynamic stability estimated in solution and predictions based on X-ray crystal structures. Secondly, the tridentate cavity seems optimum for mid-range lanthanides as previously reported for monomer **M1**[19a] and polymer **P1**^{N}.[19b] A focus on ligand **L3** indeed shows that $\beta_{1,1,\mathrm{asso}}^{\mathrm{La},\mathbf{L3}}$ = 789(26) (Ln = La) < $\beta_{1,1,\mathrm{asso}}^{\mathrm{Eu},\mathbf{L3}}$ = 4200(406) (Ln = Eu) >> $\beta_{1,1,\mathrm{asso}}^{\mathrm{Lu},\mathbf{L3}}$ = 64(4) (Ln = Lu); a peak selectivity in line with reported for triple-helical [Ln(**L1**)$_3$]$^{3+}$ complexes.[34] Its original assignment to some unfavourable inter-strand packing effect appears debatable since the same effect is now observed in 1:1 adducts where no inter-aromatic strands interaction can occur. The third trend concerns the surprising strong influence of remote substituents connected at the 5-position of the

benzimidazole ring on the stability of the final adducts [**L*k***Ln(hfa)$_3$]. The successive replacements of hydrogen atoms with weak electro-withdrawing bromine atoms along the series **L3** (no substituent) → **L4** (one Br substituent) → **L5** (two Br substituents) indeed decrease the affinity for [Ln(hfa)$_3$] by stepwise factors of two ($\beta_{1,1,\mathrm{asso}}^{\mathrm{La},\mathbf{L3}}$ = 789(26) → $\beta_{1,1,\mathrm{asso}}^{\mathrm{La},\mathbf{L4}}$ = 289(10) → $\beta_{1,1,\mathrm{asso}}^{\mathrm{La},\mathbf{L5}}$ = 116(4) and $\beta_{1,1,\mathrm{asso}}^{\mathrm{Eu},\mathbf{L3}}$ = 4200(406) → $\beta_{1,1,\mathrm{asso}}^{\mathrm{Eu},\mathbf{L4}}$ = 2718(166) → $\beta_{1,1,\mathrm{asso}}^{\mathrm{Eu},\mathbf{L5}}$ = 1306(31)). The latter trend is confirmed along the series **L2** (no substituent) → **M1** (two phenyl substituents) → **L1** (two Br substituents) with $\beta_{1,1,\mathrm{asso}}^{\mathrm{La},\mathbf{L2}}$ = 265(20) → $\beta_{1,1,\mathrm{asso}}^{\mathrm{La},\mathbf{M1}}$ = 217(2) → $\beta_{1,1,\mathrm{asso}}^{\mathrm{La},\mathbf{L1}}$ = 55(3).

The size-discriminating effect found in the monomer **L1**-**L5** (La < Eu >> Lu) also holds for the dimers **L6** and the trimer **L7** (Table 4). Interestingly, the binding units in **L6** and **L7** are connected via the 'sensitive' 5-positions of the benzimidazole rings and the affinity for the complexation of the first [Ln(hfa)$_3$] container (corrected for the available number of sites) stepwise decreases according to $\beta_{1,1,\mathrm{asso}}^{\mathrm{La},\mathbf{L3}} = 789(26) > \beta_{1,1,\mathrm{asso}}^{\mathrm{La},\mathbf{L6}}/2 = 465(9) > \beta_{1,1,\mathrm{asso}}^{\mathrm{La},\mathbf{L7}}/3 = 368(8)$ (Table 4). This trend may be at the origin of the curious decrease in affinity for [Ln(hfa)$_3$] with the length of the oligomer backbone (Figure 1b). This point merits to be rationalized with the help of the site binding model which allows to assign (i) different affinities for the binding sites if they occupy the terminal positions or the central positions in the oligomer and (ii) intersite interactions when more than one lanthanide containers are bound to the polymer backbone (Scheme 1b).

Table 3. Thermodynamic Conditional Stability Constants $\beta_{1,1,\text{asso}}^{\text{Ln},\mathbf{Lk}}$, Intrinsic Association Affinities $f_{1,1,\text{asso}}^{\text{Ln},\mathbf{Lk}}$, Thermodynamic Parameters $\Delta G_{1,1,\text{asso}}^{\text{Ln},\mathbf{Lk}} = -RT\ln\left(\beta_{1,1,\text{asso}}^{\text{Ln},\mathbf{Lk}}\right)$ and $\Delta G_{1,1,\text{asso}}^{\text{Ln},\mathbf{Lk},\infty}$, $\Delta G_{1,1,\text{asso}}^{\text{Ln},\mathbf{Lk},\text{S}}$ (eqn 8) Determined for the Titrations of Ligands **M1**, **L1-L5** with [Ln(hfa)$_3$dig] in CD_2Cl_2 + $\left|\text{dig}\right|_{\text{tot}}^{0}$ = 0.14 M at 293 K.

Ligand	**M1**	**L1**	**L2**	**L3**	**L3**	**L3**	**L4**	**L4**	**L5**	**L5**
Metal	La	La	La	La	Eu	Lu	La	Eu	La	Eu
$\beta_{1,1,\text{asso}}^{\text{Ln},\mathbf{Lk}}$	217(2)	55(3)	265(20)	789(26)	4200(406)	64(4)	289(10)	2718(166)	116(4)	1306(31)
$f_{1,1,\text{asso}}^{\text{Ln},\mathbf{Lk}}$	217(2)	55(3)	265(20)	789(26)	4200(406)	64(4)	289(10)	2718(166)	116(4)	1306(31)
$\Delta G_{1,1,\text{asso}}^{\text{Ln},\mathbf{Lk}}$ / kJ·mol^{-1}	-13.1(1)	-9.7(1)	-13.6(2)	-16.3(1)	-20.4(3)	-10.1(2)	-13.8(1)	-19.3(2)	-11.6(1)	-17.5(1)
$\Delta G_{1,1,\text{asso}}^{\text{Ln},\mathbf{Lk},\infty}$ / kJ·mol^{-1}	-13.26(2)	-8.9(1)	-12.11(1)	-17.1(1)	-21.1(7)	-10.9(1)	-12.9(2)	-20.9(3)	-10.9(1)	-16.9(3)
$\Delta G_{1,1,\text{asso}}^{\text{Ln},\mathbf{Lk},\text{S}}$ / kJ·mol^{-1}	34(4)	-177(20)	-292(20)	176(15)	212(100)	177(9)	-165(36)	223(40)	-153(18)	-80(35)

Table 4. Thermodynamic Conditional Stability Constants $\beta_{m,\mathrm{l,asso}}^{\mathrm{Ln},\mathbf{Lk}}$, Intrinsic Association Affinities $f_{\mathrm{terminal}}^{\mathrm{Ln},\mathbf{Lk}}$ and $f_{\mathrm{central}}^{\mathrm{Ln},\mathbf{Lk}}$, intersite Interactions $u_{1\text{-}2}^{\mathrm{Ln},\mathbf{Lk}}$ and Thermodynamic Parameters $\Delta G_{\mathrm{terminal}}^{\mathrm{Ln},\mathbf{Lk}} = -RT\ln\left(f_{\mathrm{terminal}}^{\mathrm{Ln},\mathbf{Lk}}\right)$, $\Delta G_{\mathrm{central}}^{\mathrm{Ln},\mathbf{Lk}} = -RT\ln\left(f_{\mathrm{central}}^{\mathrm{Ln},\mathbf{Lk}}\right)$ and $\Delta E_{1\text{-}2}^{\mathrm{Ln},\mathbf{Lk}} = -RT\ln\left(u_{1\text{-}2}^{\mathrm{Ln},\mathbf{Lk}}\right)$ Determined for the Titrations of Ligands **L6-L7** with [Ln(hfa)$_3$dig] in CD_2Cl_2 + $\left|\mathrm{dig}\right|_{\mathrm{tot}}^{0}$ = 0.14 M at 293 K.

Ligand	**L6**	**L6**	**L6**	**L7**	**L7**	**L7**
Metal	La	Eu	Lu	La	Eu	Lu
$\beta_{1,1,\mathrm{asso}}^{\mathrm{Ln},\mathbf{Lk}}$	929(17)	3730(65)	23.2(8)	1104(24)	7531(269)	82(3)
$\beta_{2,1,\mathrm{asso}}^{\mathrm{Ln},\mathbf{Lk}}$	$2.64(5)\cdot10^5$	$8.1(2)\cdot10^6$	190(6)	$7.6(2)\cdot10^5$	$2.56(9)\cdot10^7$	737(24)
$\beta_{3,1,\mathrm{asso}}^{\mathrm{Ln},\mathbf{Lk}}$	-	-	-	$3.67(8)\cdot10^7$	$8.4(3)\cdot10^9$	$1.88(6)\cdot10^4$
$f_{\mathrm{terminal}}^{\mathrm{Ln},\mathbf{Lk}}$	465(9)	1865(33)	11.6(4)	600(11)	3024(57)	10.8(8)
$f_{\mathrm{central}}^{\mathrm{Ln},\mathbf{Lk}}$	-	-	-	219(4)	1890(36)	34(2)
$u_{1\text{-}2}^{\mathrm{Ln},\mathbf{Lk}}$	1.24(2)	2.32(4)	1.43(5)	0.72(2)	0.76(1)	1.85(1)
$\Delta G_{\mathrm{terminal}}^{\mathrm{Ln},\mathbf{Lk}}$ / kJ·mol^{-1}	-14.9(2)	-18.4(4)	-5.99(9)	-15.59(5)	-19.53(5)	-5.8(2)
$\Delta G_{\mathrm{central}}^{\mathrm{Ln},\mathbf{Lk}}$ / kJ·mol^{-1}	-	-	-	-13.13(4)	-18.39(5)	-8.6(4)
$\Delta E_{1-2}^{\mathrm{Ln},\mathbf{Lk}}$ / kJ·mol^{-1}	-0.50(6)	-2.05(4)	-0.86(8)	0.84(1)	0.69(5)	-1.5(2)
AF	0.017	0.017	0.003	0.021	0.035	0.032

[a] Agreement Factor = $\mathrm{AF} = \sqrt{\sum\left(\theta_{\mathrm{Ln}}^{\mathbf{Lk},\mathrm{exp}} - \theta_{\mathrm{Ln}}^{\mathbf{Lk},\mathrm{calc}}\right)^2 \Big/ \sum\left(\theta_{\mathrm{Ln}}^{\mathbf{Lk},\mathrm{exp}}\right)^2}$.

Prediction of lanthanide loading in {P2^N[Ln(hfa)$_3$]$_m$} (m = 1 to N) metallopolymers.

Application of the site binding model (Scheme 1b-c) with the help of the tranfer matrix formalism (eqn 2) provides the binding polynomials gathered in Scheme 4,[17,18] from which the accessible thermodynamic macroconstants can be expressed for monomers **L1**-**L5** (eqn 16), dimer **L6** (eqns 17-18) and trimer **L7** (eqns 19-21) with the help of only four parameters: the intrinsic affinities for an isolated tridentate site $f_{\mathrm{asso}}^{\mathrm{Ln},\mathbf{Lk}}$, for a terminal site $f_{\mathrm{terminal}}^{\mathrm{Ln},\mathbf{Lk}}$ in the oligomer and for a central site $f_{\mathrm{central}}^{\mathrm{Ln},\mathbf{Lk}}$ in the oligomer, together with a single type of intersite interaction limited to nearest neighbours $u_{1\text{-}2}^{\mathrm{Ln}} = u_{1\text{-}2}^{\mathrm{Ln},\mathbf{L6}} = u_{1\text{-}2}^{\mathrm{Ln},\mathbf{L7}}$ operating in [**L6**(Ln(hfa)$_3$)$_2$] and in [**L7**(Ln(hfa)$_3$)$_m$] (m = 2-3).

$$\mathbf{L}\boldsymbol{k} + m\,[\mathrm{Ln(hfa)_3}] \rightleftharpoons [\mathbf{L}\boldsymbol{k}(\mathrm{Ln(hfa)_3})_m] \quad \beta^{\mathrm{Ln},\mathbf{L}\boldsymbol{k}}_{m,1,\mathrm{asso}}$$

a) Monomer (**L*k*** = **L1-L5**)

Transfer matrix: $\mathbf{T} = \begin{pmatrix} 1 & 1 \\ f^{\mathrm{Ln},\mathbf{L}\boldsymbol{k}}_{\mathrm{asso}}\left|\mathrm{Lndig}\right| & f^{\mathrm{Ln},\mathbf{L}\boldsymbol{k}}_{\mathrm{asso}}\left|\mathrm{Lndig}\right|u^{\mathrm{Ln},\mathbf{L}\boldsymbol{k}}_{1-2} \end{pmatrix}$

Partition function: $\Xi = \sum_{m=0}^{1} \beta^{\mathrm{Ln},\mathbf{L}\boldsymbol{k}}_{m,1,\mathrm{asso}} \left(\left|\mathrm{Lndig}\right|\right)^m = \begin{pmatrix}1 & 1\end{pmatrix}\mathbf{T}\begin{pmatrix}1\\0\end{pmatrix}$

$$= 1 + \underbrace{f^{\mathrm{Ln},\mathbf{L}\boldsymbol{k}}_{\mathrm{asso}}}_{\beta^{\mathrm{Ln},\mathbf{L}\boldsymbol{k}}_{1,1,\mathrm{asso}}}\left|\mathrm{Lndig}\right|$$

Macroconstants: $\beta^{\mathrm{Ln},\mathbf{L}\boldsymbol{k}}_{1,1,\mathrm{asso}}$

Microspecies: 

f_{asso}

b) Dimer (**L*k*** = **L6**)

Transfer matrix: $\mathbf{T} = \begin{pmatrix} 1 & 1 \\ f^{\mathrm{Ln},\mathbf{L}\boldsymbol{k}}_{\mathrm{terminal}}\left|\mathrm{Lndig}\right| & f^{\mathrm{Ln},\mathbf{L}\boldsymbol{k}}_{\mathrm{terminal}}\left|\mathrm{Lndig}\right|u^{\mathrm{Ln},\mathbf{L}\boldsymbol{k}}_{1-2} \end{pmatrix}$

Partition function: $\Xi = \sum_{m=0}^{2} \beta^{\mathrm{Ln},\mathbf{L}\boldsymbol{k}}_{m,1,\mathrm{asso}} \left(\left|\mathrm{Lndig}\right|\right)^m = \begin{pmatrix}1 & 1\end{pmatrix}\mathbf{T}^2\begin{pmatrix}1\\0\end{pmatrix}$

$$= 1 + \underbrace{2f^{\mathrm{Ln},\mathbf{L}\boldsymbol{k}}_{\mathrm{terminal}}}_{\beta^{\mathrm{Ln},\mathbf{L}\boldsymbol{k}}_{1,1,\mathrm{asso}}}\left|\mathrm{Lndig}\right| + \underbrace{\left(f^{\mathrm{Ln},\mathbf{L}\boldsymbol{k}}_{\mathrm{terminal}}\right)^2 u^{\mathrm{Ln},\mathbf{L}\boldsymbol{k}}_{1-2}}_{\beta^{\mathrm{Ln},\mathbf{L}\boldsymbol{k}}_{2,1,\mathrm{asso}}}\left|\mathrm{Lndig}\right|^2$$

Macroconstants: $\beta^{\mathrm{Ln},\mathbf{L}\boldsymbol{k}}_{1,1,\mathrm{asso}}$ $\beta^{\mathrm{Ln},\mathbf{L}\boldsymbol{k}}_{2,1,\mathrm{asso}}$

Microspecies: 

f_{terminal} f_{terminal}

c) Trimer (**L*k*** = **L7**)

Transfer matrices: $\mathbf{T}_{\boldsymbol{i}} = \begin{pmatrix} 1 & 1 \\ f^{\mathrm{Ln},\mathbf{L}\boldsymbol{k}}_{i}\left|\mathrm{Lndig}\right| & f^{\mathrm{Ln},\mathbf{L}\boldsymbol{k}}_{i}\left|\mathrm{Lndig}\right|u^{\mathrm{Ln},\mathbf{L}\boldsymbol{k}}_{1-2} \end{pmatrix}$ i = terminal or central

Partition function:

$$\Xi = \sum_{m=0}^{3} \beta^{\mathrm{Ln},\mathbf{L}\boldsymbol{k}}_{m,1,\mathrm{asso}} \left(\left|\mathrm{Lndig}\right|\right)^m = \begin{pmatrix}1 & 1\end{pmatrix}\mathbf{T}_{\mathbf{terminal}}\times\mathbf{T}_{\mathbf{central}}\times\mathbf{T}_{\mathbf{terminal}}\begin{pmatrix}1\\0\end{pmatrix}$$

$$= 1 + \underbrace{\left(2f^{\mathrm{Ln},\mathbf{L}\boldsymbol{k}}_{\mathrm{terminal}} + f^{\mathrm{Ln},\mathbf{L}\boldsymbol{k}}_{\mathrm{central}}\right)}_{\beta^{\mathrm{Ln},\mathbf{L}\boldsymbol{k}}_{1,1,\mathrm{asso}}}\left|\mathrm{Lndig}\right| + \underbrace{\left[\left(f^{\mathrm{Ln},\mathbf{L}\boldsymbol{k}}_{\mathrm{terminal}}\right)^2 + 2f^{\mathrm{Ln},\mathbf{L}\boldsymbol{k}}_{\mathrm{terminal}}f^{\mathrm{Ln},\mathbf{L}\boldsymbol{k}}_{\mathrm{central}}u^{\mathrm{Ln},\mathbf{L}\boldsymbol{k}}_{1-2}\right]}_{\beta^{\mathrm{Ln},\mathbf{L}\boldsymbol{k}}_{2,1,\mathrm{asso}}}\left|\mathrm{Lndig}\right|^2$$

$$+ \underbrace{\left(f^{\mathrm{Ln},\mathbf{L}\boldsymbol{k}}_{\mathrm{terminal}}\right)^2 f^{\mathrm{Ln},\mathbf{L}\boldsymbol{k}}_{\mathrm{central}}\left(u^{\mathrm{Ln},\mathbf{L}\boldsymbol{k}}_{1-2}\right)^2}_{\beta^{\mathrm{Ln},\mathbf{L}\boldsymbol{k}}_{3,1,\mathrm{asso}}}\left|\mathrm{Lndig}\right|^3$$

Macroconstants: $\beta^{\mathrm{Ln},\mathbf{L}\boldsymbol{k}}_{1,1,\mathrm{asso}}$ $\beta^{\mathrm{Ln},\mathbf{L}\boldsymbol{k}}_{2,1,\mathrm{asso}}$ $\beta^{\mathrm{Ln},\mathbf{L}\boldsymbol{k}}_{3,1,\mathrm{asso}}$

Microspecies: 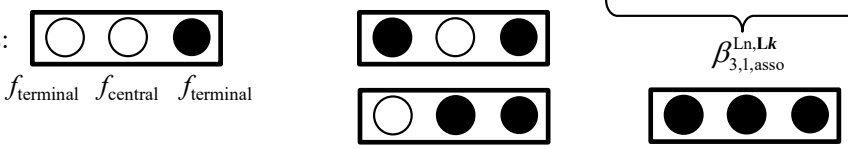

f_{terminal} f_{central} f_{terminal}

Scheme 4. Application of the site binding model for a) momomer [**L*k***Ln(hfa)3] (**L*k*** = **L1-L5**), b) dimer [**L6**(Ln(hfa)3)2] and c) trimer [**L7**(Ln(hfa)3)3] adducts (eqn 2).[17,18]

$$\beta_{1,1,\text{asso}}^{\text{Ln},\mathbf{Lk}} = f_{\text{asso}}^{\text{Ln},\mathbf{Lk}} \quad (16)$$

$$\beta_{1,1,\text{asso}}^{\text{Ln},\mathbf{L6}} = 2 f_{\text{terminal}}^{\text{Ln},\mathbf{L6}} \quad (17)$$

$$\beta_{2,1,\text{asso}}^{\text{Ln},\mathbf{L6}} = \left(f_{\text{terminal}}^{\text{Ln},\mathbf{L6}} \right)^2 u_{1\text{-}2}^{\text{Ln}} \quad (18)$$

$$\beta_{1,1,\text{asso}}^{\text{Ln},\mathbf{L7}} = 2 f_{\text{terminal}}^{\text{Ln},\mathbf{L6}} + f_{\text{central}}^{\text{Ln},\mathbf{L6}} \quad (19)$$

$$\beta_{2,1,\text{asso}}^{\text{Ln},\mathbf{L7}} = \left(f_{\text{terminal}}^{\text{Ln},\mathbf{L7}} \right)^2 + 2 f_{\text{terminal}}^{\text{Ln},\mathbf{L7}} f_{\text{central}}^{\text{Ln},\mathbf{L7}} u_{1\text{-}2}^{\text{Ln}} \quad (20)$$

$$\beta_{3,1,\text{asso}}^{\text{Ln},\mathbf{L7}} = \left(f_{\text{terminal}}^{\text{Ln},\mathbf{L7}} \right)^2 f_{\text{central}}^{\text{Ln},\mathbf{L7}} \left(u_{1\text{-}2}^{\text{Ln}} \right)^2 \quad (21)$$

For the formation of monomers [**L*k***Ln(hfa)$_3$] (**L*k*** = **L1**-**L5)**, the situation is trivial since the intrinsic binding site affinity $f_{\text{asso}}^{\text{Ln},\mathbf{Lk}}$ reflects exactly the thermodynamic association constant $\beta_{1,1,\text{asso}}^{\text{Ln},\mathbf{Lk}}$ (eqn 16), the trend of which has been discussed in the previous section (Table 3, entry 4). For the formation of the dimers [**L6**(Ln(hfa)$_3$)$_2$], again the situation is simple since eqn (17) immediately provides the intrisinc affinity $f_{\text{terminal}}^{\text{Ln},\mathbf{L6}}$ (Table 4, entry 6), while subsequent substitutions into eqn (18) give the intersite interactions $u_{1\text{-}2}^{\text{Ln}}$ (Table 4, entry 8). In line with the decrease in intrinsic affinity observed for the monomers upon connection of electron-withdrawing at the 5-position of the benzimidazole rings, the intrinsic affinity of the terminal site $f_{\text{terminal}}^{\text{Ln},\mathbf{L6}}$ in the dimer is reduced compared with that of the isolated site in the monomer $f_{\text{asso}}^{\text{Ln},\mathbf{L3}}$, by a factor 2 for Ln = La, Eu and a factor 6 for Ln = Lu. The intersite interaction is marginally cooperative ($u_{1\text{-}2}^{\text{Ln}} \geq 1$). The analysis of lanthanide loading in the trimer [**L7**(Ln(hfa)$_3$)$_m$] is more delicate because several microspecies contribute to the same macroconstants $\beta_{1,1,\text{asso}}^{\text{Ln},\mathbf{L7}}$ (eqn 19) and $\beta_{2,1,\text{asso}}^{\text{Ln},\mathbf{L7}}$ (eqn 20). A non-linear least-square fit is required, but the existence of three accessible macroscopic constants $\beta_{m,1,\text{asso}}^{\text{Ln},\mathbf{L7}}$ (m = 1-3) for fitting three unknown parameters has only minor pertinence. A reasonable way to overcome this limitation considers that $f_{\text{terminal}}^{\text{Ln},\mathbf{L6}} = f_{\text{terminal}}^{\text{Ln},\mathbf{L7}} = f_{\text{terminal}}^{\text{Ln}}$ and $u_{1\text{-}2}^{\text{Ln},\mathbf{L6}} = u_{1\text{-}2}^{\text{Ln},\mathbf{L7}} = u_{1\text{-}2}^{\text{Ln}}$ because of the structural similarities between dimer **L6** and trimer **L7**. With this in mind, a simultanous non-linear least-square fit of the five

equations (17)-(21) to the experimental macroconstants $\beta_{m,1,\text{asso}}^{\text{Ln},\mathbf{L6}}$ (m = 1-2) and $\beta_{m,1,\text{asso}}^{\text{Ln},\mathbf{L7}}$ (m = 1-3) provides the sets of optimized parameters $f_{\text{terminal}}^{\text{Ln}}$, $f_{\text{central}}^{\text{Ln}}$ and $u_{1\text{-}2}^{\text{Ln}}$ collected in Table 4, entries 6-8 (columns 5-7). For the large lanthanides (Ln = La, Eu), one observes the expected decrease in intrinsic affinity $f_{\text{terminal}}^{\text{Ln}} > f_{\text{central}}^{\text{Ln}}$ in going from the terminal site (one substituted benzimidazole ring) to the central site (two substituted benzimidazole rings), whereas very minor anti-cooperative mechanisms operate ($u_{1\text{-}2}^{\text{Ln}} \leq 1$). The opposite situation characterizes the loading of the smallest lanthanide (Ln = Lu), i.e. $f_{\text{terminal}}^{\text{Ln}} < f_{\text{central}}^{\text{Ln}}$ and $u_{1\text{-}2}^{\text{Ln}} \geq 1$. With the latter microscopic parameters in hands, the transfer matrix formalism allows to predict the binding isotherms for any oligomers $\mathbf{P2}^N$ with N binding units built from two terminal sites and N-2 central sites (Figures 7a and S22a-S23a). One starts by building the respective transfer matrices with eqn (22), from which the associated binding polynomial can be computed with eqn (23) and finally its derivation gives the target occupancy factors (eqn 24).

$$\mathbf{T}_i = \begin{pmatrix} 1 & 1 \\ f_i^{\text{Ln}} \left|\text{Lndig}\right| & f_i^{\text{Ln}} \left|\text{Lndig}\right| u_{1\text{-}2}^{\text{Ln}} \end{pmatrix} \text{ with } i = \text{terminal, central} \tag{22}$$

$$\Xi = \sum_{m=0}^{N} \beta_{m,1}^{\text{Ln},\mathbf{P2}^N} \left(\left|\text{Lndig}\right|\right)^m = \begin{pmatrix} 1 & 1 \end{pmatrix} \times \mathbf{T}_{\text{terminal}} \times \left(\mathbf{T}_{\text{central}}\right)^{N-2} \times \mathbf{T}_{\text{terminal}} \times \begin{pmatrix} 1 \\ 0 \end{pmatrix} \tag{23}$$

$$\theta_{\text{Ln}}^{\mathbf{P2}^N} = \frac{1}{N} \frac{d \ln\left(\Xi\right)}{d \ln\left(\left|\text{Lndig}\right|\right)} = \frac{1}{N} \frac{\left|\text{Ln}\right|_{\text{bound}}}{\left|\mathbf{P2}^N\right|_{\text{tot}}} = \frac{1}{N} \frac{\sum_{m=0}^{N} m \beta_{m,1}^{\text{Ln},\mathbf{P2}^N} \left(\left|\text{Lndig}\right|\right)^m}{\sum_{m=0}^{N} \beta_{m,1}^{\text{Ln},\mathbf{P2}^N} \left(\left|\text{Lndig}\right|\right)^m} \tag{24}$$

Each built binding isotherm (Figures 7a and S22a-S23a) can be then fitted with a single average affinity $f_{\text{N3}}^{\text{Ln},\mathbf{P2}^N}$ and an intersite interaction $u_{1\text{-}2}^{\text{Ln},\mathbf{P2}^N}$ by using eqn (25), as it is usually done by polymer chemists when analyzing the experimental binding isotherms of oligomers and polymers. The final trends are shown in Figures 7b and S22b-S23b.

$$\theta_{\text{Ln}}^{\mathbf{P2}^N} = \frac{1}{N} \frac{d \ln\left(\begin{pmatrix} 1 & 1 \end{pmatrix} \times \mathbf{T}^N \times \begin{pmatrix} 1 \\ 0 \end{pmatrix}\right)}{d \ln\left(\left|\text{Lndig}\right|\right)} \text{ with } \mathbf{T} = \begin{pmatrix} 1 & 1 \\ f_{\text{N3}}^{\text{Ln},\mathbf{P2}^N} \left|\text{Lndig}\right| & f_{\text{N3}}^{\text{Ln},\mathbf{P2}^N} \left|\text{Lndig}\right| u_{1\text{-}2}^{\text{Ln},\mathbf{P2}^N} \end{pmatrix} \tag{25}$$

The predicted dependence of the average intrinsic affinities with the number of sites N in $\mathbf{P2}^N$ for Ln = La (black triangles in Figure 7b) and Ln = Eu (Figure S22b) nicely reproduces the experimental data previously collected for $\mathbf{P1}^N$ (Figure 1), which finally deciphers the challenging apparent decrease in affinity when the total number of binding sites increases. The intersite interactions (red diamonds) remain almost constant.

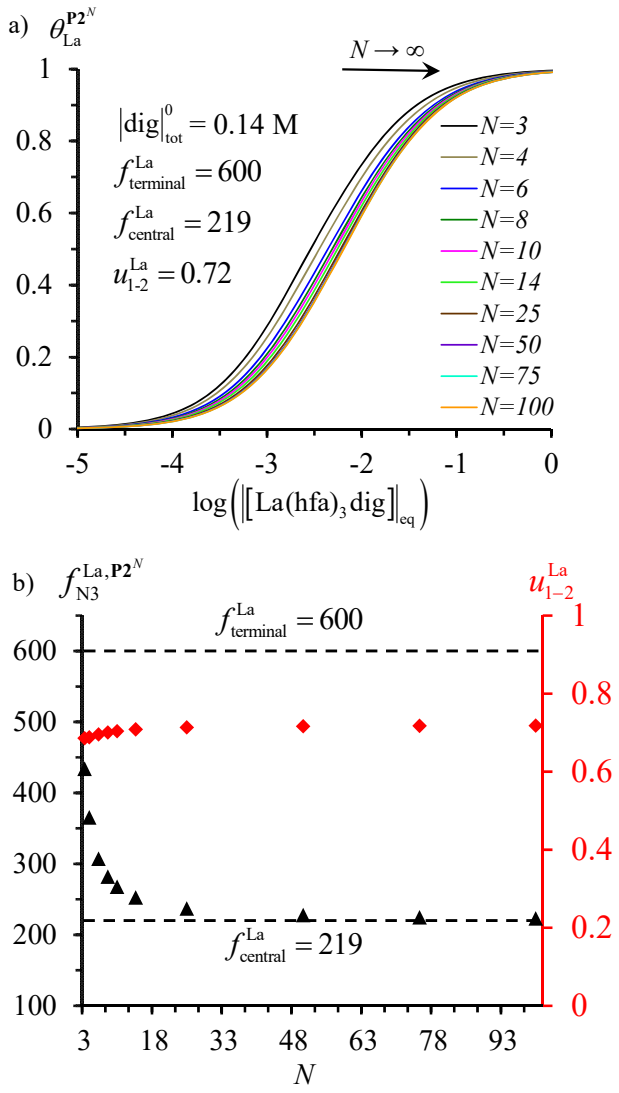

Figure 7. a) Binding isotherms predicted for $[\mathbf{P2}^N(La(hfa)_3)_m]$ in CD_2Cl_2 ($|dig|_{tot}^{0} = 0.14$ M) computed with eqns (22)-(24) and b) average intrinsic affinities $f_{N3}^{La,\mathbf{P2}^N}$ (black triangles) and intersite interactions u_{1-2}^{La} (red diamonds) obtained with eqn (25), which considers that all the binding sites have the same affinity along the linear oligomers of length N.

Conclusions

Although the tridentate 2,6-bis(benzimidazol-2-yl)pyridine scaffold was originally selected as a simple receptor displaying significant affinities for neutral lanthanide [Ln(hfa)$_3$] guests and tuneable luminescence in processable linear metallopolymers,[23] the experimental analysis of the lanthanide loading of the polymers **P1**^{N} (Figure 1b) could not be reconciled with acceptable rationalizations. A first attempt to decipher this challenge showed that the intrinsic host-guest affinities f_{N3}^{Ln} displayed (i) a concave bowl-shaped selectivity with the size of the lanthanide metal along the series[20] and (ii) some modulations of the intersite interactions $u_{1\text{-}2}^{Ln}$ with the choice of the β-diketonate co-ligands.[35] Further difficulties had to be solved concerning the variation of activity coefficients in organic solvents, prior to be able to record safe, reproducible and interpretable thermodynamic formation constants.[21,31] With this toolkit in hands, the quantitative estimation of the affinity of [Ln(hfa)$_3$] guests for the monomeric **M1**, **L1**-**L5**, dimeric **L6** and trimeric **L7** host ligands reported here confirms that (i) each tridentate binding site can accept only one lanthanide guest to give a nine-coordinate complex unit in the solid state and in solution and (ii) the significant change in activity coefficients in dichloromethane requires the use of a fixed excess of diglyme ($|dig|_{tot}^{0}$ = 0.14 M) for collecting reliable results which can be analyzed within the frame of the site binding model. We have further demonstrated that the affinity of the tridentate binding site can be logically modulated by the connection of an electron-donating alkoxy groups at the para position of the central pyridine ring in **L3**-**L5**, which significantly improves the affinity for Ln(hfa)$_3$. Some related thermodynamic effects induced by peripheral substitutions at the remote 5-position of the benzimidazole rings in **L1**, **L4** and **L5** are much more unexpected. They are at the origin of the stepwise decrease (negative power dependence) of the affinity of tridentate binding sites for the entering [Ln(hfa)$_3$] guests in linear multisite polymers of increasing lengths. In fact, each tridentate site in the polymer, except the two terminal ones, is penalized by its connection to two unfavorable electro-attractive substituents at the 5-position of the benzimidazole side arms. We are now able to predict the affinity, and consequently

the protocol for metal loading, for any oligomers with a known number of repeating units *N*. This discovery calls into question the usual procedure used by material chemists and by biologists when scanning for cooperativity while using the affinity of the isolated site in the monomer as a valuable model for the intrinsic affinity of the related site in the oligomers or in the polymers. Finally, combined with some rational programming of negative or positive cooperativity in these multisite linear receptors,[16] the current results put the basis for the selective metal loading of linear polymer **P2**^{N} for targeted applications in sensing, in light-downshifting and in light upconversion.[36]

ASSOCIATED CONTENT

Supporting Information

The Supporting Information is available free of charge at https://pubs.acs.org/doi/XXX.

Complete experimental details, ligands and complexes characterizations, NMR titrations and thermodynamic analysis (PDF).

X-ray data for **L3**-**L6** and for [**L3**Ln(hfa)$_3$] (Ln = La, Eu, Lu), [**L4**Eu(hfa)$_3$], [**L5**Eu(hfa)$_3$], [**L6**(Ln(hfa)$_3$)$_2$] (Ln = La, Eu, Yb, Lu) and [**L7**(Eu(hfa)$_3$)$_3$] (CIF).

AUTHOR INFORMATION

Corresponding Authors

Claude Piguet - *Department of Inorganic and Analytical Chemistry. University of Geneva, 30 quai E. Ansermet CH-1211 Geneva 4 (Switzerland)*. Email: Claude.Piguet@unige.ch

Authors

Mohsen Mirzakhani - *Department of Inorganic and Analytical Chemistry. University of Geneva, 30 quai E. Ansermet CH-1211 Geneva 4 (Switzerland)*.

Homayoun Nozary - *Department of Inorganic and Analytical Chemistry. University of Geneva, 30 quai E. Ansermet CH-1211 Geneva 4 (Switzerland)*.

Soroush Naseri - *Department of Inorganic and Analytical Chemistry. University of Geneva, 30 quai E. Ansermet CH-1211 Geneva 4 (Switzerland)*.

Céline Besnard - *Laboratory of Crystallography. University of Geneva, 24 quai E. Ansermet. CH-1211 Geneva 4 (Switzerland).*

Laure Guénée - *Laboratory of Crystallography. University of Geneva, 24 quai E. Ansermet. CH-1211 Geneva 4 (Switzerland).*

Notes

The authors declare no conflict of interest.

ACKNOWLEGMENTS

This work is supported through grants from the Swiss National Science Foundation (grant 200020_178758).

Dedicated to Professor Michal Borkovec for his 65th birthday.

REFERENCES

1 Morris, P. J. T. Polymer Pioneers Polymer Pioneers: A Popular History of the Science and Technology of Large Molecules. *The Beckman Center for The History of Chemistry*, University of Pennsylvania Press, 1989.

2 a) Hopff, H. Hermann Staudinger 1881–1965. *Chem. Ber.* **1969**, *102*, XLI-XLVIII; b) Mülhaupt, R. Hermann Staudinger and the Origin of Macromolecular Chemistry. *Angew. Chem. Int. Ed.* **2004**, *43*, 1054–1063.

3 McCrum, N. G.; Buckley, C. P.; Bucknall, C. B. *Principles of Polymer Engineering*. Oxford University Press, Oxford; New York, 1997.

4 a) Sjibesma, R. P.; Meijer, E. W., Self-assembly of Well-defined Structures by Hydrogen Bonding. *Curr. Opin. Colloid & Interface Sci.* **1999**, *4*, 24-32; b) de Greef, T. F. A.; Ercolani, G.; Ligthart, G. B. W. L.; Meijer, E. W.; Sijbesma, R. P., Influence of Selectivity on the Supramolecular Polymerization of AB-type Polymers Capable of both A-A and A-B Interactions. *J. Am. Chem. Soc.* **2008**, *130*, 13755-13764; c) Smulders, M. M. J.; Nieuwenhuizen, M. M. L.; de Greef, T. F. A.; van der Schoot, P.; Schenning, A. P. J. H.; Meijer, E. W., How to Distinguish Isodesmic from Cooperative Supramolecular

Polymerization. *Chem. Eur. J.* **2010**, *16*, 362-367; d) Mabesoone, M. F. J.; Palmans, A. R. A.; Meijer, E. W., Solute-Solvent Interactions in Modern Physical Organic Chemistry: Supramolecular Polymers as a Muse. *J. Am. Chem. Soc.* **2020**, *142*, 19781-19798.

5 a) Wolf, M. O., Recent Advances in Conjugated Transition Metal-Containing Polymers and Materials. *J. Inorg. Organomet. Polym. Mater.* **2006**, *16*, 189-199; b) Burnworth, M.; Knapton, D.; Rowan, S. J.; Weder, C., Metallo-Supramolecular Polymerization: a Route to Easy-to-Process Organic/Inorganic Hybrid Materials. *J. Inorg. Organomet. Polym. Mater.* **2007**, *17*, 91-103; c) Binnemans, K., lanthanide-based Luminescent Hybrid Materials. *Chem. Rev.* **2009**, *109*, 4283-4374; d) Stanley, J. M.; Holliday, B. J., Luminescent Lanthanide-containing Metallopolymers. *Coord. Chem. Rev.* **2012**, *256*, 1520-1530; e) Winter, A.; Schubert, U. S., Synthesis and Characterization of Metallo-supramolecular Polymers. *Chem. Soc. Rev.* **2016**, *45*, 5311-5357; f) Wang, Y.; Astruc, D.; Abd-El-Aziz, A. S., Metallopolymers for Advanced Sustainable Applications. *Chem. Soc. Rev.* **2019**, *48*, 558-636.

6 a) Kido, J.; Okamoto, Y., Organo-Lanthanide Metal Complexes for Electroluminescent Materials. *Chem. Rev.* **2002**, *102*, 2357-2368; b) Chen, X.-Y.; Yang, X.; Holliday, B. J., Photoluminescent Europium-Containing Inner Sphere Conducting Metallopolymer. *J. Am. Chem. Soc.* **2008**, *130*, 1546-1547; c) Ho, C.-L.; Wong, W.-Y., Metal-Containing Polymers: Facile Tuning of Photophysical Traits and Emerging Applications in Organic Electronics and Photonics. *Coord. Chem. Rev.* **2011**, *255*, 2469-2502; Morais, A.; Bernardo, D. R.; Germino, J. C.; Nogueira, A. F.; Freitas, J. N., Photo and Electroluminescence of a Phenylene Vinylene Conjugated Polymer Containing Bipyridine Units and Chelated Europium Complex. *J. Luminesc.* **2021**, *230*, 117764.

7 a) Huang, X.; Han, S.; Huang, W.; Liu, X., Enhancing Solar Cell Efficiency: the Search for Luminescent Materials as Spectra Converters. *Chem. Soc. Rev.* **2013**, *42*, 173-201; b) Bünzli, J.-C. G.; Chauvin, A.-S., Lanthanides in Solar Energy Conversion. *Handbook on the Physics and Chemistry of Rare Earths*, Bünzli, J.-C. G.; Pecharsky, V. K., Eds. Elsevier North

Holland: Amsterdam, **2014**; *44*, 169-281; c) Hasegawa, Y., Photofunctional Lanthanoid Complexes, Coordination Polymers, and Nanocrystals for Future Photonic Applications. *Bull. Chem. Soc. Jpn* **2014**, *87*, 1029-1057.

8 a) Binnemans, K.; van Deun, R.; Görller-Walrand, C.; Haase, W.; Bruce, D. W.; Malykhina, L.; Galyametdinov, Y. G., Anisotropic Molecular Magnetic Materials Based on Liquid-Crystalline Lanthanide Complexes. *Mater. Science and Eng.* **2001**, *C18*, 247-254; b) Andruh, M.; Costes, J.-P.; Diaz, C.; Gao, S., 3d-4f Combined Chemistry: Synthetic Strategies and Magnetic Properties. *Inorg. Chem.* **2009**, *48*, 3342-3359; c) Vaz, M. G. F.; Andruh, M., Molecule-Based Magnetic Materials Constructed from Paramagnetic Organic Ligands and two Different Metal Ions. *Coord. Chem. Rev.* **2021**, *427*, 213611.

9 a) De Bettencourt-Dias, A.; Rossini, J. S. K., Ligand Design for Luminescent Lanthanide-Containing Metallopolymers. *Inorg. Chem.* **2016**, *55*, 9954-9963; b) Zhang, Z.; He, Y.-N.; Liu, L.; Lü, X.-Q.; Zhu, X.-J.; Wong, W.-K.; Pan, M.; Su, C.-Y., Pure White-Light and Colour-Tuning of Eu^{3+}-Gd^{3+}-Containing Metallopolymer. *Chem. Commun.* **2016**, *52*, 3713-3716.

10 a) Kuriki, K.; Koike, Y.; Okamoto, Y., Plastic Optical Fiber Lasers and Amplifiers Containing Lanthanide Complexes. *Chem. Rev.* **2002**, *102*, 2347-2356; b) Sloof, L. H.; van Blaaderen, A.; Polman, A.; Hebbink, G. A.; Klink, S. I.; Van Veggel, F. C. J. M.; Reinhoudt, D. N.; Hofstraat, J. W., Rare-Earth Doped Polymers for Planar Optical Amplifiers. *J. Appl. Phys.* **2002**, *91*, 3955-3980; c) Mech, A.; Monguzzi, A.; Meinardi, F.; Mezyk, J.; Macchi, G.; Tubino, R., Sensitized NIR Erbium(III) Emission in Confined Geometries: a New Strategy for Light Emitters in Telecom Applications. *J. Am. Chem. Soc.* **2010**, *132*, 4574-4576.

11 a) Vanden Bussche, F.; Kaczmarek, A. M.; Schmidt, J.; Stevens, C. V.; Van Der Voort, P., Lanthanide Grafted Phenanthroline-Polymer for Physiological Temperature Range Sensing. *J. Mater. Chem. C* **2019**, *7*, 10972-10980; b) Vanden Bussche, F.; Kaczmarek, A. M.; Van

Speybroeck, V.; Van Der Voort, P.; Stevens, C. V., Overview of N-Rich Antennae Investigated in Lanthanide-Based Temperature Sensing. *Chem. Eur. J.* **2021**, *27*, 7214-7230.

12 a) Rehahn, M., Organic/Inorganic Hybrid Polymers. *Acta Polym.* **1998**, *49*, 201-224; b) *Macromolecule-Metal Complexes*, eds. F. Ciardelli, E. Tsuchida, D. Wöhrle, Springer Verlag, Berlin, 1996.

13 Wolf, M. O., Transition-Metal-Polythiophene Hybrid Materials. *Adv. Mater.* **2001**, *13*, 545-553.

14 a) de Bettencourt-Dias, A., Lanthanide-based Emitting Materials in Light-Emitting Diodes. *Dalton Trans.* **2007**, 2229-2241; b) Hatanaka, M.; Hirai, Y.; Kitagawa, Y.; Nakanishi, T.; Hasegawa, Y.; Morokuma, K., Organic Linkers Control the Thermosensitivity of the Emission Intensities from Tb(III) and Eu(III) in a Chameleon Polymer. *Chem. Sci.* **2017**, *8*, 423-429.

15 a) Cook, T. R.; Zheng, Y.-R.; Stang, P. J., Metal-Organic Frameworks and Self-Assembled Supramolecular Coordination Complexes: Comparing and Contrasting the Design, Synthesis, and Functionality of Metal-Organic Materials. *Chem. Rev.* **2012**, *113*, 734-777; b) Cui, Y.; Yue, Y.; Qian, G.; Chen, B., Luminescent functional metal-Organic Frameworks. *Chem. Rev.* **2012**, *112*, 1126-1162; c) Heine, J.; Müller-Buschbaum, K., Engineering Metal-Based Luminescence in Coordination Polymers and Metal-Organic Frameworks. *Chem. Soc. Rev.* **2013**, *42*, 9232-9242; d) Mahata, P.; Mondal, S. K.; Singha, D. K.; Majee, P., Luminescence Rare-Earth-Based MOFs as Optical Sensors. *Dalton Trans.* **2017**, *46*, 301-328; e) Dzhardimalieva, G. I.; Uflyand, I. E., Design and Synthesis of Coordination Polymers with Chelated Units and their Application in Nanomaterials Science. *RSC Adv.* **2017**, *7*, 42242-42288; f) Yin, H. Q.; Yin, X. B., Metal-Organic Frameworks with Multiple Luminescence Emissions: Designs and Applications. *Acc. Chem. Res.* **2020**, *53*, 485-495; g) Gorai, T.; Schmitt, W.; Gunnlaugsson, T., Highlights of the Development and Application of

Luminescent Lanthanide Based Coordination Polymers, MOFs and Functional Nanomaterials. *Dalton Trans.* **2021**, *50*, 770-784.

16 Babel, L.; Baudet, K.; Hoang, T. N. Y.; Nozary, H.; Piguet, C., A Rational Approach to Metal Loading of Organic Multi-Site Polymers: Illusion or Reality. *Chem. Eur. J.* **2018**, *24*, 5423-5433.

17 a) Borkovec, M.; Jönsson, B.; Koper, G. J. M., Ionization Processes and Proton Binding in Polyprotic Systems: Small Molecules, Proteins, Interfaces and Polyelectrolytes. *Colloid Surface Sci.*, **2001**; *16*, 99-339; b) Garcés, J. L.; Koper, G. J. M.; Borkovec, M., Ionization Equilibria and Conformational Transitions in Polyprotic Molecules and Polyelectrolytes. *J. Phys. Chem. B.* **2006**, *110*, 10937-10950; c) Koper, G. J. M.; Borkovec, M., Proton Binding by Linear, Branched, and Hyperbranched Polyelectrolytes. *Polymer* **2010**, *51*, 5649-5662; d) Borkovec, M.; Cakara, D.; Koper, G. J. M., Resolution of Microscopic Protonation Enthalpies of Polyprotic Molecules by Means of Cluster Expansions. *J. Phys. Chem. B* **2012**, *116*, 4300-4309.

18 a) Koper, G.; Borkovec, M., Binding of Metal Ions to Polyelectrolytes and their Oligomeric Counterparts: an Application of a Generalized Potts Model. *J. Phys. Chem. B* **2001**, *105*, 6666-6674; b) Borkovec, M.; Hamacek, J.; Piguet, C., Statistical Mechanical Approach to Competitive Binding of Metal Ions to Multi-Center Receptors. *Dalton Trans.* **2004**, 4096-4105; c) Borkovec, M.; Koper, G. J. M.; Piguet, C., Ion Binding to Polyelectrolytes. *Curr. Opinion in Coll. and Int. Science* **2006**, *11*, 280-289; d) Hamacek, J.; Borkovec, M.; Piguet, C., Simple Thermodynamics for Unravelling Sophisticated Self-Assembly Processes. *Dalton Trans.* **2006**, 1473-1490.

19 a) Babel, L.; Hoang, T. N. Y.; Nozary, H.; Salamanca, J.; Guénée, L.; Piguet, C., Lanthanide Loading of Luminescent Multi-Tridentate Polymers under Thermodynamic Control. *Inorg. Chem.* **2014**, *53*, 3568-3578: b) Hoang, T. N. Y.; Wang, Z.; Babel, L.; Nozary, H.; Borkovec,

M.; Szilagyi, I.; Piguet, C., Metal Loading of Lanthanidopolymers Driven by Positive Cooperativity. *Dalton Trans.* **2015**, *44*, 13250-13260.

20 Babel, L.; Hoang, T. N. Y.; Guénée, L.; Besnard, C.; Wesolowski, T. A.; Humbert-Droz, M.; Piguet, C., Looking for the Origin of Allosteric Cooperativity in Metallopolymers. *Chem. Eur. J.* **2016**, *22*, 8113-8123.

21 Baudet, K.; Kale, V.; Mirzakhani, M.; Babel, L.; Naseri, S.; Besnard, C.; Nozary, H.; Piguet, C., Neutral Heteroleptic Lanthanide Complexes for Unravelling Host-Guest Assemblies in Organic Solvents: The Law of Mass Action Revisited. *Inorg. Chem.* **2020**, *59*, 62-75.

22 a) Preston, P. N., Synthesis, Reactions, and Spectroscopic Properties of Benzimidazoles. *Chem. Rev.* **1974**, *74*, 279-314; b) Piguet, C.; Bocquet, B.; Hopfgartner, G., Syntheses of Segmental Heteroleptic Ligands for the Self-Assembly of Heteronuclear Helical Supramolecular Complexes. *Helv. Chim. Acta* **1994**, *77*, 931-942; c) McKenzie, B. M.; Miller, A. K.; Wojtecki, R. J.; Johnson, J. C.; Burke, K. A.; Tzeng, K. A.; Mather, P. T.; Rowan, S. J., Improved Synthesis of Functionalized Mesogenic 2,6-Bisbenzimidazolepyridine Ligands. *Tetrahedron* **2008**, *64*, 8488-8495.

23 Zaïm, A.; Nozary, H.; Guénée, L.; Besnard, C.; Lemonnier, J.-F.; Petoud, S.; Piguet, C., N-Heterocyclic Tridentate Aromatic Ligands Bound to [Ln(hfa)$_3$] Units: Thermodynamic, Structural and Luminescent Properties. *Chem. Eur. J.* **2012**, *18*, 7155-7168.

24 a) Semmelhack, M. F.; Helquist, P. M.; Jones, L. D., Synthesis with Zerovalent Nickel - Coupling of Aryl Halides with Bis(1,5-Cyclooctadiene)Nickel(0). *J. Am. Chem. Soc.* **1971**, *93*, 5908-5910.; b) Yamamoto, T.; Wakabayashi, S.; Osakada, K., Mechanism of C-C Coupling Reactions of Aromatic Halides, Promoted by Ni(CoD)2 in the Presence of 2,2'-Bipyridine and PPh3, to Give Biaryls. *J. Organomet. Chem.* **1992**, *428*, 223-237.; c) Constable, E. C.; Morris, D.; Carr, S., Functionalised 3,3'-Bipyridine - a New Class of Dinucleating Ligands. *New J. Chem.* **1998**, 287-294; d) Asakura, H.; Shishido, T.; Tanaka,

T., In Situ Time-Resolved XAFS Study of the Reaction Mechanism of Bromobenzene Homocoupling Mediated by [Ni(COD)(bpy)]. *J. Phys. Chem. A* **2012**, *116*, 4029-4034.

25 a) Ueda, M.; Saitoh, A.; Ohtani, S.; Miyaura, N., Synthesis of Biaryls via Nickel-Catalyzed Cross-Coupling Reaction of Arylboronic Acids and Aryl Mesylates. *Tetrahedron* **1998**, *54*, 13079-13086; b) Tobisu, M.; Chatani, N., Devising Boron Reagents for Orthogonal Functionalization through Suzuki-Miyaura Cross-Coupling. *Angew. Chem. Int. Ed.* **2009**, *48*, 3565-3568; c) Amatore, C.; Le Duc, G.; Jutand, A., Mechanism of Palladium-Catalyzed Suzuki-Miyaura Reactions: Multiple and Antagonistic Roles of Anionic Base and their Counter-Cations. *Chem. Eur. J.* **2013**, *19*, 10082-10093.

26 Grein, F., Twist Angles and Rotational Energy Barriers of Biphenyl and Substituted Biphenyls. *J. Phys. Chem. A* **2002**, *106*, 3823-3827.

27 a) SHAPE is a free software developed by Llunell, M; Casanova, D.; Cirera, J.; Alemany, P.; Alvarez, S. and available online at http://www.ee.ub.edu/; b) Pinsky, M.; Avnir, D., Continuous Symmetry Measures. 5. The Classical Polyhedral. *Inorg. Chem.* **1998**, *37*, 5575-5582; c) Casanova, D.; Cirera, J.; Llunell, M.; Alemany, P.; Avnir, D.; Alvarez, S. Minimal Distortion Pathways in Polyhedral Rearrangements. *J. Am. Chem. Soc.* **2004**, *126*, 1755-1763; d) Alvarez, S., Polyhedra in (Inorganic) Chemistry. *Dalton Trans.* **2005**, 2209-2233.

28 a) Brown, I. D.; Altermatt, D., Bond-Valence Parameters Obtained from a Systematic Analysis of the Inorganic Crystal-Structure Database. *Acta Cryst. B* **1985**, *41*, 244-247; b) Brese, N. E.; Okeeffe, M., Bond-Valence Parameters for Solids. *Acta Cryst. B* **1991**, *47*, 192-197; c) Brown, I. D., Chemical and Steric Constraints in Inorganic Solids. *Acta Cryst. B* **1992**, *48*, 553-572; d) Brown, I. D., *The Chemical Bond in Inorganic Chemistry*, Oxford University Press, UK, 2002; e) Brown, I. D., Recent Development in the Methods and Applications of the Bond Valence Model. *Chem. Rev.* **2009**, *109*, 6858-6919; f) Escande, A.; Guénée, L.; Buchwalder, K.-L.; Piguet, C., Complexation of Trivalent Lanthanides with Planar Tridentate Aromatic Ligands Tuned by Counteranions and Steric Constraints. *Inorg. Chem.* **2009**, *48*,

1132-1147; g) Trzesowska, A.; Kruszynski, R.; Bartczak, T. J., New Bond-Valence Parameters for Lanthanides. *Acta Cryst. B* **2004**, *60*, 174-178; h) Trzesowska, A.; Kruszynski, R.; Bartczak, T. J., New Lanthanide-Nitrogen Bond-Valence Parameters. *Acta Cryst. B* **2005**, *61*, 429-434.

29 Smith, M. B.; March, J. *March's Advanced Organic Chemistry*, 6th Ed, Wiley-Interscience, New Jersey, 2009, 404.

30 Freund, C.; Porzio, W.; Giovanella, U.; Vignali, F.; Pasini, M.; Destri, S.; Mech, A.; Di Pietro, S.; Di Bari, L.; Mineo, P., Thiophene Based Europium *β*-Diketonate Complexes: Effect of the Ligand Structure on the Emission Quantum Yield. *Inorg. Chem.* **2011**, *50*, 5417-5429.

31 Baudet, K.; Guerra, S.; Piguet, C., Chemical Potential of the Solvent: A crucial Player for Rationalizing Host-Guest Affinities. *Chem. Eur. J.* **2017**, *23*, 16787-16798.

32 Gokcen, N. A., Gibbs-Duhem-Margules Laws. *J. Phase Equilibria* **1996**, *17*, 50-51.

33 a) Castellano, B. M.; Eggers, D. K., Experimental Support for a Desolvation Energy Term in Governing Equations for Binding Equilibria. *J. Phys. Chem. B* **2013**, *117*, 8180-8188; b) Eggers, D. K.; Fu, S.; Ngo, D. V.; Vuong, E. H.; Brotin, T., Thermodynamic Contribution of Water in Cryptophane Host-Guest Binding Reaction. *J. Phys. Chem. B* **2020**, *124*, 6585-6591.

34 Petoud, S.; Bünzli, J.-C. G.; Renaud, F.; Piguet, C.; Schenk, K. J.; Hopfgartner, G., Stability and Size-Discriminating Effects in Mononuclear Lanthanide Triple Helical Building Blocks with Tridentate Aromatic Ligands. *Inorg. Chem.* **1997**, *36*, 5750-5760.

35 Babel, L.; Guénée, L.; Besnard, C.; Eliseeva, S. V.; Petoud, S.; Piguet, C., Cooperative Loading of Multisite Receptors with Lanthanide Containers: an Approach for Organized Luminescent Metallopolymers. *Chem. Sci*. **2018**, *9*, 325-335.

36 a) Suffren, Y.; Golesorkhi, B.; Zare, D.; Guénée, L.; Nozary, H.; Eliseeva, S. V.; Petoud, S.; Hauser, A.; Piguet, C., Taming Lanthanide-Centered Upconversion at the Molecular Level. *Inorg. Chem.* **2016**, *55*, 9964-9972; b) Charbonnière, L. J., Bringing Upconversion Down to the Molecular Scale. *Dalton Trans.* **2018**, *47*, 8566-8570; c) Golesorkhi, B.; Nozary, H.;

Fürstenberg, A.; Piguet, C., Erbium Complexes as Pioneers for Implementing Linear Light-Upconversion in Molecules. *Mater. Horiz.* **2020**, *7*, 1279-1296; d) Nonat, A. M.; Charbonnière, L. J., Upconversion of Light with Molecular and Supramolecular Lanthanide Complexes. *Coord. Chem. Rev.* **2020**, *409*, 213192; e) Healy, C.; Hermanspahn, L.; Kruger, P. E., Photon Upconversion in Self-Assembled Materials. *Coord. Chem. Rev.* **2021**, *432*, 213756.

TOC

The tridentate 2,6-bis(benzimidazole)pyridine binding units acts as a tunable host for binding lanthanide tris-β-diketonates guests [Ln(hfa)$_3$]. A large size-discriminating effect is observed for mid-range lanthanides while the host-guest affinity changes with the number of binding sites forming the linear oligomeric receptors.